NATIONAL ADVISORY COMMITTEE FOR AERONAUTICS

TECHNICAL NOTE 3567

STUDY OF SCREECHING COMBUSTION IN A 6-INCH SIMULATED AFTERBURNER

By Perry L. Blackshear, Warren D. Rayle, and Leonard K. Tower

Lewis Flight Propulsion Laboratory
Cleveland, Ohio

Washington

October 1955

NATIONAL ADVISORY COMMITTE FOR AERONAUTICS

TECHNICAL NOTE 3567

STUDY OF SCREECHING COMBUSTION IN A 6-INCH SIMULATED AFTERBURNER

By Perry L. Blackshear, Warren D. Rayle, and Leonard K. Tower

SUMMARY

As part of a general research program on screeching combustion at the NACA Lewis laboratory, an investigation was conducted to develop screech instrumentation and to study the mechanism of screech in a 6-inch-diameter simulated afterburner.

Probe microphones were developed that can be utilized to measure the frequency, relative amplitude, and relative phasing of the pressure oscillations at various positions within a screeching combustor. In calibrating these microphones to determine absolute values of pressure amplitude, a new theory was proposed to account for the nonlinear attenuation of high-amplitude sound in tubes.

The acoustic oscillations accompanying screech in the 6-inch afterburner consisted of the first transverse (sloshing) mode in the hot gases downstream of the flameholder.

INTRODUCTION

The trend toward higher flight speeds for military aircraft creates the need for jet engines of increased thrust. The trend in afterburner and ram-jet combustor development has therefore been toward combustors that operate at higher pressures, higher combustion temperatures, and higher velocities. With the development of these high-output combustors, the phenomenon known as screech has been widely encountered throughout the aircraft industry. Screech derives its name from the high-pitched audible sound accompanying the phenomenon. Other manifestations of screech are high-frequency pressure oscillation in the combustor and an increased rate of heat transfer, which have resulted in rapid deterioration or failure of combustor shell, flameholder, and other combustor parts. In most instances, therefore, screech is undesirable and is to be avoided. It is essential that an understanding of the screech phenomenon be obtained and that a method of controlling or eliminating screech be devised.

Screech has received some detailed study in rocket (refs. 1 and 2), simulated ram-jet (ref. 3), and afterburning (ref. 4) engines. In references 1, 2, and 4, screech was identified as a transverse mode of oscillation by comparing the experimentally observed frequency with the frequencies calculated from the various acoustic modes possible in an idealized chamber resembling the combustors employed. In reference 3, screech was identified as a transverse mode by schlieren pictures of the motion of the flame near the flameholder and by inspection of the frequency obtained. A more detailed study of the screech mechanism is desirable, since (1) a wide assortment of idealized modes can give evidence similar to that reported in references 1 to 4, and (2) conditions within the combustors suggest a much more complicated picture of the oscillation than the idealized acoustic treatment admits (ref. 5).

The investigation reported herein, which is part of a general program to investigate screech at the NACA Lewis laboratory, had a two-fold objective: (1) to develop suitable instrumentation for studying screech in an operating combustor, and (2) to make the measurements of screech necessary to assess the screech mechanism. The investigation was conducted with a 6-inch-diameter direct-connect combustor. The combustor configuration and operating conditions simulated a turbojet afterburner. The instrumentation, which was developed and evaluated for studying screech, included a probe microphone capable of measuring the pressure fluctuations at any point within the combustor. This permitted a detailed study of the spatial distribution of amplitudes, frequencies, and relative phases. Ionization gaps were utilized to indicate the position of the flame front in the vicinity of the flameholder. In order to calibrate the probe microphone, an experimental and theoretical investigation was made of the attenuation of large-amplitude sound in tubes.

From surveys of the screech-amplitude distribution, frequency, and relative phasing, the oscillatory motion of the gases in the combustor was deduced by comparing the experimental results with phemomena predicted from theoretical consideration of various modes of acoustic oscillation. A limited study was made of the effect on screech amplitude and frequency of such system variables as combustor pressure, air-flow rate, fuel-air ratio, and flameholder type and position.

The work reported herein was conducted during 1952-53, and has been reported with additional information in an NACA classified document.

APPARATUS AND PROCEDURE

Installation

A diagram of the combustor installation is shown in figure 1. The inlet and outlet ducts were connected to the laboratory air supply and exhaust systems. Air-flow rates and combustor pressures were regulated by a remote-controlled valve upstream of the combustor and by a variable-area combustor exhaust nozzle. A tubular production-model turbojet

combustor was installed in the duct upstream of the research combustor to provide conditions in the inlet stream simulating conditions at the inlet of a turbojet afterburner.

Research Combustor

The research combustor (fig. 2) had an inside diameter of 6 inches and a length (measured from the position of the flameholder to the position of the exhaust nozzle) that could be varied from 34 to $45\frac{3}{4}$ inches by traversing the flameholder. The flameholder was traversed axially by means of a wire cable and a winch. The combustor having the variable-area exhaust nozzle and the water-jacketed combustor shell shown in figure 2 was used for only a part of the investigation reported herein; during the early phases of this investigation, the combustor had a fixed-area exhaust nozzle and an air-cooled outer shell. Fuel, JP-4 or gasoline, was supplied to the combustor through an air-atomizing spray bar (fig. 3) located 100 inches upstream of the exhaust nozzle at the position indicated in figure 1. Four flameholders were investigated: two single diametric V-type flameholders $1\frac{1}{2}$ and $2\frac{1}{4}$ inches wide and two 60°-single-cone flameholders with area blockages of 30 and 46 percent.

3070

General Instrumentation

Air flow was metered by a concentric-hole, sharp-edged orifice installed according to A.S.M.E. specifications. Fuel flow was metered by a calibrated rotameter. Combustor-inlet pressure was measured by four wall static taps as indicated in figure 1. Combustor-inlet temperature was measured by chromel-alumel thermocouples connected to a self-balancing recording potentiometer. A thrust target was employed to measure the momentum of the exhaust. This was later replaced by a water quench spray, followed by a thermocouple array. The rise in enthalpy across the system then indicated the thermal efficiency.

Special Instrumentation

Microphone probe development. - An instrument was required that could be used to measure the frequency and amplitude of the pressure oscillations accompanying screech and to determine the pressure distribution of any standing wave system in the combustor. To determine the pressure distribution, two basic techniques were apparent: (1) move the sensing element to various positions in the combustor, or (2) utilize a movable probe to pick up the pressure signal at various locations and transmit this signal to the sensing element located outside the combustor. There exist water-cooled pressure pickups that can withstand limited exposure to flame when mounted on the combustor wall. The life of these pickups is in constant jeopardy with designs employed so far, and to adapt these pickups to immersion in the hot gas stream would hardly seem feasible.

Therefore, probe microphones for measuring the frequency and relative amplitude of screech in an operating combustor were designed, fabricated, and subjected to preliminary evaluation by measuring screech in the 6-inch-diameter simulated afterburner. The instruments showing the greatest promise were then selected for more detailed calibration and additional studies of screech. The necessary calibration consisted of a measurement of the attenuation of pressure waves between the open end of the probe and the microphone.

Description of instruments. - The probe microphone is shown in figure 4. A water-cooled probe that could be traversed diametrically through the combustor was connected to a 50-foot coil of 1/4-inch copper tubing that behaved acoustically as an infinite tube in that it produced negligible reflection of pressure pulses entering the tube. The sensing element, a microphone, was connected to this "infinite" tube by a short 1/32-inch-diameter lead at a point near the combustor. To prevent combustion gases containing soot and moisture from entering the probe during normal operation, a small flow of clean, dry air was maintained through the "infinite" tube into the combustor. The air purge was not adequate to keep the tube completely clean, since rapid changes in combustor operating conditions caused pressure surges that sometimes carried combustion gases into the tube. To avoid changes in the tube attenuation constants resulting from soot deposited from these combustion gases, it was deemed necessary to use a tube of reasonably large diameter (3/16-in. I.D.).

Special probes were fabricated to check the reliability of the phase measurements obtained with the standard probe microphone. These "phase" probes were intended primarily to produce reliable phase measurements; the reliability of their amplitude readings was assumed to be small. A diagram of such a probe is shown in figure 5. The distance from the end of the probe to the microphone was minimized to avoid variations in internal phase lag. The bore of the tube was kept small to enable viscous damping to minimize the effect of reflected waves. An ample supply of cooling water was passed through the jacket of the probes, keeping the gas within the small tube at a temperature above the dewpoint of the combustion products.

Readings obtained with the phase probes confirmed the validity of the phase measurements made with the standard probe microphone. The phase measurements are therefore presented under RESULTS AND DISCUSSION without qualification as to the instrument employed.

Calibration. - In order to calibrate the special screech instruments for frequency and amplitude response, the apparatus shown in figure 6 was utilized. The apparatus for generating low-amplitude pressure waves (fig. 6(a)) consisted of a resonance chamber driven by a piston speaker. The apparatus for high-amplitude pressure waves (fig. 6(b)) consisted of

a similar resonance chamber driven by a high-pressure air jet that was admitted intermittently by a rotating "chopper" disk. The readings of the research instruments were compared with the readings of a reference microphone that had previously been calibrated with a known steady-state variation in pressure. From these data the attenuation coefficient for the probe microphone was computed.

A theoretical analysis was made of the damping of high-amplitude pressure waves, and the resulting theoretical equations were utilized to correlate the experimental data on attenuation of high-amplitude waves. Theoretical considerations were also utilized to correct for the change in amplitude accompanying the transmission of a pressure wave across a temperature interface such as that existing between the hot gases in the combustor and the cold purge air flowing through the probe microphone.

Attenuation of Low-Amplitude Sound in Tubes

The attenuation and distortion of periodic pressure waves in tubes must be considered in designing and calibrating the probe microphone. The apparatus shown in figure 6(a) was utilized to measure attenuation constants for low-amplitude pressure waves and for various probe lengths. The so-called Kirchoff attenuation constant α_k for 1/4-inch tubes was computed from the relation

$$\alpha_k = \frac{\ln \frac{p_1}{p_2}}{x_2 - x_1} \tag{1}$$

where the symbols have the meanings listed in appendix A. The experimental values obtained from equation (1) were approximately 15 percent greater than the theoretical Kirchoff value; the data are presented in figure 7.

Attenuation of High-Amplitude Sound in Tubes

Screech oscillations having a peak-to-peak pressure amplitude as great as 20 inches of mercury have been encountered. For such pressure oscillations the magnitude of the attenuation coefficient is reported to be dependent on the amplitude (refs. 6 to 8). Since these references do not agree on the shape of the attenuation-against-amplitude curve, the data contained in the references were not considered adequate for computing the damping of high-frequency, high-amplitude waves in the 1/4-inch tube. An experimental and theoretical investigation of the damping of high-frequency, high-amplitude pressure waves in small tubes was therefore undertaken as part of this investigation.

Theoretical. - A derivation of equations describing various factors affecting the behavior of high-amplitude sound in tubes is given in appendix B. The factors can be briefly summarized as follows:

The sound pressure in the entrance of the probe is related to that of the source by the equation

$$p_r - p_e = \frac{5}{14} p_e^2 \tag{2}$$

It is well-known (ref. 9) that high-amplitude sound waves propagating in free air tend to develop a saw-tooth wave form; that is, the waves generate higher harmonics. The amplitude below which the n^{th} harmonic of a wave of frequency f will not grow is

$$p_{max} \cong \frac{0.292\ c\alpha n^m(n-1)}{f(n+1)} \tag{3}$$

where

0.292 depends on $\gamma = 1.4$

α damping constant for fundamental component

m exponent of f in α ($\alpha = \alpha' f^m$)

In free air $m = 2$ and α is rather small for the frequencies of primary interest. For viscous damping in tubes, m is $1/2$; and, if α is defined as $\alpha'\sqrt{f}$, equation (3) becomes

$$p_{max} \cong 0.292\ c\alpha' \sqrt{\frac{n}{f}} \frac{(n-1)}{(n+1)} \tag{4}$$

For the case where this value is exceeded for the first several harmonics, the length of propagation for a sound wave to become saw-toothed is

$$x^* \cong \ln \left(\frac{p_{e,max}}{p_{e,max} - 0.292\lambda\alpha_k} \right)^{\frac{1}{\alpha_k}} \tag{5}$$

If the amplitude-dependent attenuation coefficient is defined as

$$-\frac{\frac{dp_{max}}{dx}}{p_{max}} = \alpha_p \tag{6}$$

3070

this constant can be expressed as

$$\alpha_p = \frac{12f}{a}\left[\left(1 + p_{max}\right)^{\frac{1}{7}} - 1\right] \qquad (7)$$

(again for $\gamma = 1.4$).

A plot of equation (7) is presented in figure 8. Values of the amplitude-dependent damping coefficient α_p were combined with the experimental values of the Kirchoff damping coefficient α_k, and the resulting expression for the combined damping effects was integrated to obtain the curves shown in figure 9, where values of p_{max} are plotted as a function of tube length x for three frequencies. Figure 9 indicates that even for high amplitudes the Kirchoff damping has a rather large effect in determining the over-all attenuation.

Therefore, the factors affecting a high-amplitude wave as it enters and propagates in the tube are as follows: First the amplitude is reduced on entering the tube according to equation (2). If the wave form is sinusoidal, it will become saw-toothed after propagating a distance given by equation (5), during which time it is attenuated by Kirchoff damping (eq. (1)). Once the wave becomes saw-toothed, it is attenuated according to the integrated equation shown in figure 9. Consideration of these factors yields the theoretical curves shown in figure 10.

Experimental. - Figure 11 shows the wave form recorded at 1080 cycles per second for various tube lengths in the probe microphone using the apparatus of figure 6(b). From these wave forms and from simultaneous voltmeter readings, the mean-to-peak amplitudes were determined.

Figure 12 presents a comparison of the pressure amplitude indicated by the probe microphone with that indicated by the calibrated reference microphone for frequencies of 1080, 2400, and 3000 cycles per second. Also presented in figure 12 are the theoretical values of figure 10. Values of α_p obtained from the curves of figure 12 are compared in figure 13 with the theoretical values from figure 8. Also shown in figure 13 are values of α_p obtained from references 6 and 8.

Discussion. - From the foregoing results it is seen that probe microphones used in measuring high-amplitude, high-frequency sound become less sensitive as the probe length is increased and as the wavelength decreases. Fortunately, observed screech frequencies tend to decrease as combustor diameter is increased (e.g., ref. 4). The resulting design principle is fairly obvious; for maximum sensitivity of the probe microphone, the distance from the end of the probe to the microphone should be kept small. It is possible to obtain a reasonably accurate picture of the wave form by the use of a probe microphone only if the wave travels less than a distance x^* as defined in equation (5).

The agreement between the observed and computed nonlinear attenuation coefficient is surprisingly good. If calibration facilities are not available, these values may be used for computing the amplitude-dependent attenuation until some more refined method becomes available.

References 6 to 8 postulate turbulence as the cause of the nonlinear attenuation of high-amplitude sound in tubes. Figure 13 shows that the theoretical nonlinear damping coefficients derived in appendix B are in reasonable agreement with both the experimental values of references 6 to 8, which were obtained in large tubes, and the experimental values obtained in this investigation with 1/4-inch tubes. Consequently, it appears that α_p is independent of tube size and hence is not a direct function of Reynolds number. The theory presented in appendix B is therefore believed to afford a better explanation of the observed nonlinear attenuation.

3070

Effect of Temperature Discontinuity on Probe-Microphone Reading

All the foregoing effects have been for an assumed constant mean temperature. When the gas temperature within the probe differs from the temperature in the combustor, a reflection will take place where the sound wave enters the tube. Assuming that particle displacement and sound pressure are equal on either side of this interface, the ratio of the transmitted wave to the incident wave amplitudes can be computed as a function of the temperature ratio of the gas on either side of this interface. This ratio is given in the following equation:

$$\frac{p_{tr}}{p_{inc}} = \frac{2}{1 + \sqrt{\frac{T_{tr}}{T_{inc}}}} \tag{8}$$

Flame Detection

Ionization gaps were used to detect the local motions of the flame during screech and to give an indication of particle motion in a combustor. The ionization gaps used are shown in figure 14. The use of these gaps coupled with a surface-mounted pressure pickup provided an instantaneous picture of the relation between the local pressure and the flame-front position near a flameholder.

Several variations of photocell probes were made and tried. The results were not satisfactory. A periodic variation in the luminosity of the flame zone downstream of the flameholder was obtained with the photocell probe sketched in figure 15. This probe consisted of a small periscope purged with clean, dry air flowing through the periscope into the combustor. The photocell recorded an integrated value of the light

emitted within a narrow cone between the periscope and the wall. The photocell probe produced a periodic signal during screech and therefore shows promise; it has not been used sufficiently, however, to warrant its recommendation. The ionization gaps, on the other hand, which were simpler to construct and to operate, have given very interesting data and are recommended for further screech investigations.

Procedure

The relative screech amplitude at various positions across the diameter of the 6-inch afterburner was measured at different distances downstream of the flameholder. The distance between the flameholder and the probe microphone was varied by changing the axial position of the flameholder. The pressure amplitude at the wall of the combustor was measured at 18 points along the length of the combustor by leaving the flameholder fixed and moving the microphone to the various positions of measurement. During the process of making these surveys of relative screech amplitude, the frequency spectrum of the sound was also recorded at various positions in the combustor.

The relative phasing of the pressure signal at different positions in the combustor was determined with two microphone pickups. Phase measurements were made between a reference pressure signal and the pressure signal obtained in vertical diametric surveys at three distances downstream of the flameholder ($\frac{3}{4}$, 4, and $7\frac{1}{2}$ in.). Phase relations were also measured at 18 points along the length of the combustor. With two ionization gaps located 180° apart, 3/4 inch downstream of the flameholder, and extending 3/4 inch from the burner walls, oscillations of the flame were detected. Simultaneous measurements with the ionization gaps and a microphone pickup were used to determine the relative phasing between the flame position and the pressure in the combustor.

The peak-to-peak pressure amplitude was measured at various pressures and air-flow rates in the 6-inch afterburner. At each of several air-flow rates the combustor pressure was progressively lowered to determine the limiting pressure below which screech was not encountered. Measurements of screech amplitude and frequency were made at various fuel-air ratios in the combustor; these data were obtained with the fixed-area exhaust nozzle, however, and changes in fuel-air ratio were accompanied by variations in combustor-inlet velocity and combustor pressure.

RESULTS AND DISCUSSION

Screech Mechanism

Amplitude distribution. - The relative screech amplitude at various positions across the combustor diameter is shown in figure 16 for surveys made at different distances downstream of the flameholder. The data of figure 16 were obtained by traversing the flameholder axially along the length of the combustor. At certain locations of the flameholder in the combustor, the longitudinal mode of oscillation would sometimes appear, and the indicated unfiltered amplitude of screech would rise. Figure 17 shows an oscilloscope trace of a combined intense low-frequency note with screech and a phase relation of the two frequencies obtained with appropriate band-pass filters. There is an apparent modulation of the screech amplitude by the low-frequency note. For most positions of the flameholder, the 3300-cycle screech constituted the dominant oscillation. For other positions, however, the low-frequency 490-cycle oscillation was dominant, as indicated in figure 16. Figure 18 shows typical spectra of sound recorded at the combustor wall for both the low- and high-frequency oscillations.

In all surveys shown in figure 16 where the 3300-cycle oscillation was dominant, the amplitude exhibits a pronounced dip near the center of the duct. This is the amplitude pattern to be expected with a transverse mode of oscillation, as shown in figure 19. Such a pattern could not result from radial or longitudinal oscillations.

Figure 20 shows a comparison of a sound spectrum at the combustor wall with a spectrum at the center of the duct for conditions producing the amplitude dip at the center. Only the high-frequency part of the spectrum (3300 cps) is attenuated at the center. It is concluded, therefore, that the frequency associated with the transverse mode is about 3300 cycles per second. The data shown in figures 16, 17, 18, and 20 are raw data taken with 3 feet of transmission line piping the signal to the microphone and subject to the corrections previously discussed.

For two positions of the flameholder, the amplitude at the wall was measured at 18 points along the length of the combustor with a single microphone moved from point to point to obtain the data shown in figure 21. These data show a peak in the screech amplitude about 5 inches downstream of the flameholder. This peak lies in the region where the maximum heat-release rate might be expected.

The circumferential distribution of sound at a plane $1\frac{1}{2}$ inches downstream of a V-gutter flameholder is shown in figure 22. These data were gathered in three successive tests, the flameholder being rotated 45° between tests. The filtered screech signal is plotted against position relative to the gutter. A strong maximum is apparent at locations

perpendicular to the gutter, thus indicating that the gutter orientation controls the direction of the transverse oscillation. Also plotted is the higher-frequency content of the signal; this, too, is minimum behind the gutter but does not demonstrate so marked a peak as the screech fundamental. This may be interpreted as suggesting a nonsinusoidal driving force which acts over a relatively large portion of the cross section.

The data presented in figures 16, 21, and 22 are considered conclusive evidence that the screech oscillation studied comprised a standing transverse wave. The circumferential and radial distribution follows the general shape demanded by such a wave; the longitudinal survey may also be so interpreted. The amplitude peak shown on figure 21 does not indicate the presence of a standing longitudinal wave; rather it signifies the location from which the transverse oscillation is driven. If a combined longitudinal and transverse mode existed, the frequency would be

$$f = \frac{c}{2}\sqrt{\left(\frac{n_z}{l}\right)^2 + \left(\frac{2\beta}{d}\right)^2} \tag{9}$$

where n_z/l is the reciprocal of the half wavelength of the longitudinal oscillations, and d is the burner diameter (ref. 10). If this longitudinal component is to have an appreciable effect on the indicated frequencies, the half wavelength would have to be of the order of a diameter. With a half wavelength of this magnitude, multiple pressure nodes would occur in the 38-inch length surveyed. Since multiple nodes are not evidenced in figure 21, there exist no longitudinal components which can appreciably affect the frequency. The screech frequency can therefore be expressed by the relation

$$f = \frac{c\beta}{d} \tag{10}$$

The values of β (ref. 10) for the first two pure transverse modes of oscillation are 0.568 and 0.972.

Frequency. - The observed screech frequency of approximately 3300 cycles per second can be produced by the first pure transverse mode of oscillation ($\beta = 0.568$) if the speed of sound is 2920 feet per second, or by the second transverse mode ($\beta = 0.972$) if the speed of sound is 1710 feet per second. These values for the speed of sound correspond to average temperatures of 3850° and 1250° R, respectively. The higher of these temperatures approaches the theoretical flame temperature; the lower approaches the temperature of the inlet air. Consideration of screech frequency therefore indicates that the oscillation could consist of the first transverse mode in the hot gas or the second transverse mode in the inlet stream. For transverse modes of oscillation, the pressure will be out of phase on the opposite sides of the combustor for

odd modes and in phase on opposite sides of the combustor for even modes of oscillation, along any diameter except an antinodal diameter. Phase measurements should therefore make it possible to determine whether the first or the second transverse mode of oscillation occurs.

Phase measurements. - By means of the special phase probes, vertical diametric surveys of pressure amplitude were made at three distances downstream of the flameholder ($\frac{3}{4}$, 4, and $7\frac{1}{2}$ in.) to obtain the data shown in figures 23 and 24. A typical oscilloscope trace is shown in figure 23. The phase of the pressure signal relative to the signal obtained 3/4 inch downstream of the flameholder at the top wall of the combustor is indicated in figure 24. The 180° phase shift across a diameter indicates that the first transverse mode rather than the second mode of oscillation persisted in the combustor. The data of figures 23 and 24 indicate that there is also a phase shift along the length of the combustor. The relative phase of the pressure signal along the top of the combustor is shown in figure 21. These data also indicate the existence of a pronounced phase shift in the vicinity of the flameholder, signifying that in this region the waves have longitudinal components. The absence of a phase shift in the hot gases downstream of the flameholder indicates the existence of pure transverse oscillation in this region.

Circumferential phase relations were sought. The results were not conclusive and could be interpreted as evidence either of standing or traveling transverse oscillation according to the desire of the interpreter. This may be attributed to the large separation (90°) of the instrumentation positions, to the nonsinusoidal nature of the wave, or to a phase lag between the driving force and the oscillation.

With two ionization gaps located 180° apart, 3/4 inch downstream of the flameholder and extending 3/4 inch from the burner walls, the signals shown in figure 25(a) were obtained. The flame striking the ionization gaps was 180° out of phase on opposite sides of the combustor. At positions farther downstream a random component was superimposed on the periodic component, making the signal difficult to interpret.

Simultaneous measurements of pressure and flame-produced ionization at a station 3/4 inch downstream of the flameholder (fig. 25(b)) showed that the outward flame-front motion is in phase with the pressure at this station. On the basis of these phase measurements, a time sequence of events in the screech cycle can be constructed as shown in figure 26. The relation between the pressure and the flame-front displacement is precisely that which would accompany a transverse oscillation.

3070

Effect of System Variables on Screech

Pressure. - The effect of pressure on screech amplitude is shown in figure 27. The peak-to-peak pressure amplitude showed a general increase with increase in combustor pressure. These measurements were made with a flush-mounted microphone located upstream of the flameholder and therefore do not represent the maximum values of amplitude (see fig. 21). The air-flow rate is noted for each data point in figure 27. At an air-flow rate of 1.5 pounds per second, the pressure limit for screech was 20 inches of mercury. Detailed measurements were not made of variations in frequency with pressure; sufficient observation was made, however, to ascertain that no marked change in frequency occurred as pressure was varied.

Through-flow. - The combustor screeched throughout most of its operating range, as shown in figure 28. Screech was encountered at progressively lower pressures as through-flow was decreased. During screech the combustion efficiency was 90 to 100 percent; the efficiency dropped abruptly by approximately 35 percent when screech ceased.

The limited data of figure 27 show no consistent variation of screech amplitude with variation in flow rate. No effect of flow rate on screech frequency was noted for the limited range investigated; these data are presented in table I. These tests were conducted with a fixed-area exhaust nozzle, however, and the maximum variation in combustor-inlet velocity was about 20 percent.

Fuel-air ratio. - The effect on screech of variations in fuel-air ratio is shown by the data of table I. The fixed-area nozzle was used to obtain these data; this did not permit changes in fuel-air ratio without simultaneous variations in combustor-inlet velocity and combustor pressure. Only qualitative trends can therefore be noted. Fuel-air ratio exhibited no pronounced effect on screech amplitude. The effect of fuel-air ratio on screech frequency was as follows. Maximum frequency of 3500 cycles per second was obtained at an equivalence ratio of 1.146. Screech frequency decreased as fuel-air ratio was decreased below this value. The frequency was 3350 cycles per second at an equivalence ratio of 0.934 and 2800 cycles per second near the lean blow-out limit. When the fuel throttle valve was abruptly closed, combustion persisted for one to two seconds. During this time the screech frequency continuously declined to a value much lower than 2800 cycles per second.

Flameholder type. - Two single diametric V-type flameholders and two 60° single-cone flameholders were investigated. With the V-type flameholders, an aperiodic roughness was obtained that was superimposed on the high-frequency screech. The larger V-type flameholder burned out after 20 minutes of operation. The flameholders giving greater area blockage permitted a wider fuel-air-ratio range of operation. All the flameholders investigated screeched throughout most of their operating range of fuel-air ratio.

Flameholder position. - No appreciable change in screech frequency or amplitude was noticed when the flameholder position was altered to produce combustor lengths from 34 to 45 inches. At one position of the flameholder (giving a combustor length of 42 in.), however, a longitudinal mode of oscillation having a frequency of approximately 470 cycles per second appeared. This longitudinal oscillation did not replace the screech but merely accompanied and modulated it as shown in figure 17.

Speculation Regarding Screech Mechanism

The data thus far indicate that the gas in the burner does, in fact, execute a transverse oscillation during screech. Little has been said, however, of the means whereby the oscillation is maintained. Some source of energy is obviously required. Two sources of energy are available in the combustor: (1) the kinetic energy in the flowing gas stream, and (2) the chemical energy released during the combustion process. Of these two sources, the chemical energy is far greater. In order that this energy be made available to overcome damping and maintain the oscillations at a high amplitude, it is necessary for it to be involved in some time-varying work cycle. The criterion proposed by Rayleigh (ref. 11) is that the heat input should occur at locations where the pressure varies and at a time when the pressure is near its maximum. For a case where the oscillations are driven by the kinetic energy of the flowing stream, the heat release may play a part in intermittently storing and releasing this kinetic energy in such a manner that the oscillation is maintained (ref. 12). In either event, it is obvious that the oscillation may be driven only when the heat release undergoes a variation with time. This may be brought about in many ways.

A coupling between the chemical reaction and the acoustic oscillations could result from the effect of pressure and temperature on the chemical kinetics. The rate of energy release per unit volume in high-speed combustion equipment has been shown to increase with increase in pressure and temperature (ref. 13). A relation of this sort can be used to predict the variation in heat-release rate resulting from an adiabatic compression of the burning gases. A similar result obtains if the combustion zone is assumed to comprise many laminar flames again subjected to adiabatic compression. Both approaches indicate an amount of energy available for driving the oscillation that is proportional to the mean local heat-release rate and to the square of the dimensionless perturbation pressure.

Such an approximation was applied to the experimental burner reported herein. At typical conditions, perturbation pressure of 0.5, the available energy was found to be about 3 percent of the total energy in the fuel supplied.

The oscillation is damped, its energy removed, in at least four ways: (1) sound propagation upstream, (2) mass transport downstream, (3) absorption and scattering at the outer wall, and (4) nonlinear damping of the waves in the manner discussed in appendix B.

Damping of types (1) to (3) depends on amplitude squared. Type (4) damping is a function of amplitude cubed. The rate of energy loss due to (1) and (2) for the experimental burner was estimated to be from one-third to one-half the rate at which energy would be supplied. Damping of type (3) becomes of comparable magnitude only when the walls are made highly dissipative. The nonlinear attenuation (type (4)) is significant only when the amplitude is large.

The foregoing crude picture enables the following predictions to be made as to the variation of screech tendency with operational parameters. The dimensionless amplitude p would be an index of the difference between the driving power and the "linear" damping terms (1) to (3); hence, it would serve as an index of screech tendency. This tendency will increase with increases in mass flow, inlet temperature, flameholder blockage, and mean heat-release rate. The tendency will increase with pressure only if the local heat-release rate per pound per second also rises. If the dimensionless amplitude p is constant, the amplitude $P - P_{av}$ will increase linearly with pressure. These general predictions seem to be in agreement with the experimental findings.

The previous concept of damping and driving assumes the heat release to be in phase with the pressure. If this is not true, the driving force would be reduced. Also neglected were the possible roles of flame wrinkling and detonation. A flame-front disturbance, possibly caused by the scattering of waves at the flameholder, certainly exists, as evidenced by the excellent schlieren photographs of reference 3 and by the data shown in figure 25. The resultant time-varying heat release may well be an important constituent of the driving force.

It is quite possible that in the environment of the screeching combustor, the heat-release rate may at times more nearly approach that of detonation rather than that associated with steady conflagration. This again could alter the energy driving the oscillation. Neither of the last-mentioned factors, however, would alter drastically the trends predicted by the use of the simplified picture.

There are certain beneficial aspects of screech. One of these is the increased combustion efficiency accompanying screech. Another is the possible gain in the over-all heat cycle for a given thermal efficiency. This can occur because most of the heat is released at a higher level of pressure with screech. It is uncertain how much of this excess energy is available above that required to overcome damping of the oscillation. To retain the beneficial aspects of screech while minimizing the destructive effects would demand a thorough and quantitative evaluation of control techniques.

SUMMARY OF RESULTS

The results of an investigation to develop instrumentation and study screech in a 6-inch-diameter simulated afterburner can be summarized as follows:

1. Probe microphones were developed that can be utilized to measure the frequency, relative amplitude, and phase relations of pressure oscillations at various positions within a screeching combustor.

2. Calibration data were obtained that make possible the determination of the absolute value of pressure amplitude from probe-microphone readings. In obtaining these calibration data, a new theory was proposed to account for the nonlinear attenuation of high-amplitude sound in tubes.

3. From measurements of pressure-amplitude distribution, frequency, and relative phasing during screeching operation of a 6-inch-diameter simulated afterburner, the acoustic oscillations accompanying screech were found to consist of the first transverse (sloshing) mode in the hot gases downstream of the flameholder.

4. The small-scale afterburner investigated screeched throughout most of its operating range. Screech was absent only at conditions approaching flame blow-out; screech disappeared just before blow-out as pressure was decreased or as air flow was increased.

Lewis Flight Propulsion Laboratory
National Advisory Committee for Aeronautics
Cleveland, Ohio, October 1, 1953

APPENDIX A

SYMBOLS

The following symbols are used in this report:

a	mean sound velocity relative to the gas, ft/sec
c	local sound velocity relative to the gas, ft/sec
d	combustor diameter, ft
f	frequency, sec^{-1}
n	integer denoting particular harmonic
P	local pressure, lb/sq in. abs
P_{av}	mean pressure, lb/sq in. abs
p	perturbation pressure, $(P/P_{av}) - 1$
t^*	time required for a wave to become saw-toothed, sec
u	local gas velocity relative to fixed coordinates, ft/sec
V	propagation velocity of saw-tooth shock front relative to fixed coordinates, ft/sec
v	wave-propagation velocity, relative to fixed coordinates, ft/sec
x	distance, ft
x^*	distance required for a wave to become saw-toothed, ft
α	damping coefficient, ft^{-1}
α_e	effective over-all damping coefficient, $\alpha_e = \alpha_k + \alpha_p$, ft^{-1}
α_k	viscous damping coefficient, ft^{-1}
α_p	saw-tooth damping coefficient, ft^{-1}
α'	damping coefficient for wave of unit frequency, $\alpha' = \alpha/f^m$, ft^{-1}
β	constant
λ	wavelength, c/f, ft

Subscripts:

e	conditions obtained at probe entrance
max	conditions obtained at wave maximum pressure
min	conditions obtained at wave minimum pressure
n	integer denoting particular harmonic
r	conditions obtained at sound source

APPENDIX B

DISTORTION AND DIMINUTION OF SOUND WAVES OF FINITE AMPLITUDE IN TUBES

It has been established (ref. 9) that finite-amplitude sound waves tend toward a saw-tooth wave form as they propagate. A portion of a single saw-tooth wave has been examined in reference 14, which showed that, up to pressure ratios of 2.5, the sound speed computed by the isentropic relation

$$\frac{c}{a} = (1 + p)^{\frac{1}{7}} \tag{B1}$$

differs by less than 1 percent from that determined from the Rankine-Hugoniot relation

$$\frac{c}{a} = \left[\frac{(1 + p)(7 + p)}{1 + 6(1 + p)}\right]^{\frac{1}{2}} \tag{B2}$$

(when $\gamma = 1.4$). Also the Riemann invariant

$$Q \equiv 5c - u = \text{constant} \tag{B3}$$

was found to vary less than 1 percent for shocks up to $P/P_{av} = 2.5$ (i.e., $p = 1.5$).

Since Q is constant for rarefaction waves and approximately constant for shock waves, equations (B1) and (B3) define the relation between u, c, and p.

From the foregoing considerations, a number of useful relations can be derived for the propagation of sound in tubes.

End effect. - At high sound levels, the variation in static pressure at the entrance of the tube will not be equal to the pressure variation in the medium from which the impulse is taken. This results from the assumptions that (1) wave energy is conserved and (2) the incident sound has no particle velocity component in the direction of the tube. With these assumptions the energy equation reads

$$u_e^2 + 5c_e^2 = 5c_r^2 \tag{B4}$$

Within the tube, the speed of sound and the particle velocity are related by the equation

$$5c_e - u_e = 5a \tag{B3}$$

The speed of sound may be related to sound pressure by

$$\frac{c}{a} = (1 + p)^{\frac{1}{7}} \approx 1 + \frac{p}{7} \tag{B1}$$

3970

Combining equations (B1), (B3), and (B4) yields the following expression relating the sound pressure in the probe entrance with that in the source:

$$p_r - p_e \approx \frac{5}{14} p_e^2 \tag{2}$$

Transition to saw-tooth. - A harmonic distortion of finite sound waves results from the variation in sound speed between the compressed and the rarefied portions of the wave, as indicated by equation (B1). Thus, any finite wave, regardless of its initial form, will approach more and more closely the saw-toothed shape as time passes; that is, the leading portion of the wave will become a shock wave, while the rarefaction will become more and more gradual. The rate at which this transition occurs will, of course, depend on the magnitude of the wave.

If a train of sine waves be engendered in an initially stationary medium, the waves will become saw-tooth in form in a time

$$t^* = \frac{\lambda}{4(v_{max} - a)} \tag{B5}$$

Since

$$v_{max} = c_{max} + u_{max} \tag{B6}$$

equations (B1), (B3), (B5), and (B6) may be combined to give

$$t^* = \frac{7\lambda}{24ap_{max}} \tag{B7}$$

The distance the wave travels during transition is then

$$x^* = \frac{7\lambda}{24p_{max}} \tag{B8}$$

These relations should apply to waves propagating in ideal gases. If the waves are confined in a tube, the factor of viscous damping must be considered. The ideal saw-tooth wave may be represented by the Fourier expansion

$$p = \frac{2p_{max}}{\pi} \sum_{n=1}^{\infty} \frac{(-1)^{n+1}}{n} \sin 2\pi fn\left(\frac{x}{c} - t\right) \tag{B9}$$

Since the viscous damping increases with increasing frequency, a physical wave may more truly be represented by terminating the series with the n^{th} harmonic. The finite series will then exhibit a pressure maximum at a point

$$x' = \frac{\lambda}{2} \frac{n}{n+1} \tag{B10}$$

if ft in equation (B9) is set equal to an integer.

If the damping of the n^{th} harmonic of a wave of frequency f follows the relation

$$p_n = p_{n,e}^{-\alpha' f^m n^m x} \tag{B11}$$

the rate of decay of p_n with distance is

$$\frac{dp_n}{dx} = - p_n \alpha' f^m n^m \tag{B12}$$

Assuming a uniform rate of growth of this harmonic, equations (B8) and (B10) yield

$$\frac{dp_n}{dx} = \frac{p_n p_{max}}{\frac{7\lambda}{24} \frac{n-1}{n+1}} \tag{B13}$$

The value of p_{max} below which p_n will no longer grow is found by equating the sum of equations (B12) and (B13) to zero, yielding

$$p_{max} \cong \frac{0.292\alpha n^m (n-1)c}{(n+1)f} \tag{3}$$

In free air $m = 2$ and α is small for the frequencies of interest. In fairly small tubes, m is $1/2$; when $\alpha = \alpha' \sqrt{f}$, equation (3) becomes

$$p_{max} = \frac{0.292c\alpha' \sqrt{n}(n-1)}{\sqrt{f}(n+1)} \tag{4}$$

If the viscous (Kirchoff) damping coefficient is applied to the wave during the transition from sine to saw-tooth by the relation

$$p_{max} = p_{e,max} e^{-\alpha_k x} \tag{B14}$$

the transition time and distance can be recalculated by the use of

$$at_n^* + \frac{\lambda}{4}\frac{n-1}{n+1} = \int_0^{t_n^*} v_{max}\, dt \tag{B15}$$

This becomes, by equations (B1), (B3), (B6), (B14), and (B15),

$$t_n^* = \frac{1}{\alpha_k a} \ln \frac{24p_{e,max}\, a\,(n+1)}{-7\lambda\alpha_k(n-1) + 24p_{e,max}(n+1)} \tag{B16}$$

or

$$x_n^* = at_n^* = \frac{1}{\alpha_k} \ln \frac{24p_{e,max}(n+1)}{24p_{e,max}(n+1) - 7\lambda\alpha_k(n-1)} \tag{B17}$$

or, for large n,

$$x^* = \frac{1}{\alpha_k} \ln \frac{p_{e,max}}{p_{e,max} - 0.292\lambda\alpha_k} \tag{5}$$

Nonlinear attenuation. - If the original pressure wave is of sufficient amplitude to generate a large number of harmonics, a nonlinear attenuation results. This occurs as a result of the overriding of the shock front by the following rarefaction impulse. In considering this attenuation it is assumed that the wave will remain approximately saw-tooth in form and that the mean pressure will be found halfway between the maximum and the minimum pressures. The Rankine-Hugoniot equation

$$\frac{u_{max} - u_{min}}{c_{min}} = \frac{5}{6}\left(\frac{V-u_{min}}{c_{min}} - \frac{c_{min}}{V-u_{min}}\right) \tag{B18}$$

may be written in quadratic form and solved as follows:

$$V = 0.6\, u_{max} + 0.4\, u_{min} + \sqrt{0.36(u_{max} - u_{min})^2 + c_{min}^2} \tag{B19}$$

Equations (B1) and (B3) may be combined to give

$$u = 5a\left[(1 + p)^{\frac{1}{7}} - 1\right] \cong 5a\left(\frac{p}{7} - \frac{3}{49}\,p^2\right) \tag{B20}$$

which, with equation (B19) and the assumption of equal pressure and rarefaction magnitudes, gives

$$\frac{V}{a} \cong \frac{p_{max}}{7}\left(1 - \frac{15}{7}\,p_{max}\right) + \sqrt{1 - \frac{2}{7}\,p_{max} + \frac{31}{49}\,p_{max}^2} \cong 1 \tag{B21}$$

Thus, it is seen that little error would be introduced by assuming that the propagation velocity of the shock front is equal to the speed of sound in the undisturbed medium.

The rate at which the saw-tooth wave diminishes because of the overriding of the rarefaction upon the shock front can be expressed in terms of a nonlinear damping coefficient α_p, defined as

$$\alpha_p = -\frac{1}{p_{max}}\frac{dp_{max}}{dx} = -\frac{1}{ap_{max}}\frac{dp_{max}}{dt} \tag{6}$$

The equivalent expression, in terms of peak and average wave velocities, is

$$\alpha_p = \frac{2}{a\lambda}\,(v_{max} - a) \tag{B21}$$

which may be combined with equations (B1), (B3), and (B6) to give

$$\alpha_p = \frac{12f}{a}\left[(1 + p_{max})^{\frac{1}{7}} - 1\right] \tag{7}$$

This nonlinear damping is assumed to be accompanied by viscous damping; the effective damping coefficient for saw-tooth waves in a tube is taken as the sum of the two effects:

$$\alpha_e = \alpha_p + \alpha_k = \frac{12f}{a}\,(1 + p_{max})^{\frac{1}{7}} + \alpha_k - \frac{12f}{a} \tag{B22}$$

The variation of peak pressure with distance can then be obtained by integration, again using the binomial expansion of $(1 + p_{max})^{1/7}$ and discarding terms of higher order than p_{max}^2. This yields the expression

$$\alpha_e = \frac{-dp_{max}}{p_{max}\,dx} \cong \frac{12}{7}\frac{f}{a}\left(p_{max} - \frac{3}{7}p_{max}^2\right) + \alpha_k \qquad \text{(B23)}$$

from which

$$\int \frac{dp_{max}}{p_{max}\left[\frac{12f}{7a}\left(p_{max} - \frac{3}{7}p_{max}^2\right) + \alpha_k\right]} = -\int dx \qquad \text{(B24)}$$

or

$$e^{-2\alpha_k x} = \frac{C_o p_{max}^2}{\frac{12f}{7a}\left(p_{max} - \frac{3}{7}p_{max}^2\right) + \alpha_k}\left(\frac{1 - \frac{6}{7}p_{max} + \sqrt{1 + \frac{a\alpha_k}{f}}}{1 - \frac{6}{7}p_{max} - \sqrt{1 + \frac{a\alpha_k}{f}}}\right)^{\frac{1}{\sqrt{1 + \frac{a\alpha_k}{f}}}} \qquad \text{(B25)}$$

where C_o is the constant of integration. For a given frequency and tube size, this equation may be plotted as in figure 9.

To summarize, there are three regions with distinct characteristics through which the sound wave travels in a probe-type microphone; the entrance, the transition region, and the saw-tooth region. Considering these regions separately, curves may be drawn for a given probe diameter that will represent the internal sound level as a function of source level and tube length. The sound level at the tube entrance is less than that of the source by the amount indicated from equation (2). During the transition (the length of this region is determined from eq. (5)), the linear (Kirchoff) damping coefficient applies (eq. (B14)). When the transition is complete, the damping coefficient of equation (B23) must be used. Such a set of curves is shown in figure 10.

3070

REFERENCES

1. Smith, R. P., and Sprenger, D. F.: Combustion Instability in Solid-Propellant Rockets. Fourth Symposium (International) on Combustion, The Williams & Wilkins Co., 1953, pp. 893-906.

2. Ross, Chandler C., and Datner, Paul P.: A Monograph on the Problem of Combustion Instability in Liquid-Propellant Rocket Motors. Paper presented at meeting Am. Rocket Soc., New York (N.Y.), Nov. 30-Dec. 3, 1954.

3. Kaskan, W. E., and Noreen, A. E.: High-Frequency Oscillations of a Flame Held by a Bluff Body. A.S.M.E. Trans., vol. 77, no. 6, Aug. 1955, pp. 885-891; discussion, pp. 891-895.

4. Truman, John C., and Newton, Roger T.: Why Do High-Thrust Engines Screech? Aviation Age, vol. 23, no. 5, May 1955, pp. 136-143.

5. Moore, Franklin K., and Maslen, Stephen H.: Transverse Oscillations in a Cylindrical Combustion Chamber. NACA TN 3152, 1954.

6. Lehmann, K. O.: Die Dämpfungsverluste bei starken Schallschwingungen in Rohren. Annalen der Physik, Folge 5, Bd. 21, Dec. 1934, pp. 533-552.

7. Binder, R. C.: The Damping of Large Amplitude Vibrations of a Fluid in a Pipe. Jour. Acous. Soc. Am., vol. 15, no. 1, July 1943, pp. 41-43.

8. Richardson, E. G.: The Damping of Sound Waves of Large Amplitude in Tubes. Proc. Math. and Phys. Soc. of Egypt, vol. 3, no. 3, 1947.

9. Fay, R. D.: Plane Sound Waves of Finite Amplitude. Jour. Acous. Soc. Am., Oct. 1931, pp. 222-241.

10. Morse, Philip M.: Vibration and Sound. McGraw-Hill Book Co., Inc., 1936.

11. Rayleigh: Theory of Sound. Vol. II. Dover Pub., 1945.

12. Blackshear, Perry L., Jr.: Driving Standing Waves by Heat Addition. NACA TN 2772, 1952.

13. Childs, J. Howard, McCafferty, Richard J., and Surine, Oakley W.: Effect of Combustor Inlet Conditions on Performance of an Annular Turbojet Combustor. NACA Rep. 881, 1947. (Supersedes NACA TN 1357.)

14. Chandrasekhar, S.: On the Decay of Plane Shock Waves. Rep. No. 423, Ballistic Res. Labs., Aberdeen Proving Ground (Maryland), 1953.

TABLE I. - OBSERVED FREQUENCIES FOR SIMULTANEOUS VARIATIONS OF MASS FLOW, EQUIVALENCE RATIO, AND BURNER PRESSURE

[Inlet-gas temperature, 1660° R]

Frequency, cps	Mass flow, lb/sec	Equivalence ratio	Mean pressure, P_{av}, lb/sq in.	Inlet velocity, ft/sec
3350	2.005	0.9339	19.78	310.9
3500	2.080	1.104	20.78	307.1
3500	2.080	1.146	20.78	307.1
3400	1.990	.9968	20.28	301.0
3400	2.452	1.007	22.28	337.6
3400	2.787	.9964	24.28	352.1
3400	3.166	.9881	26.28	369.6
3350	3.474	.9595	28.28	376.8

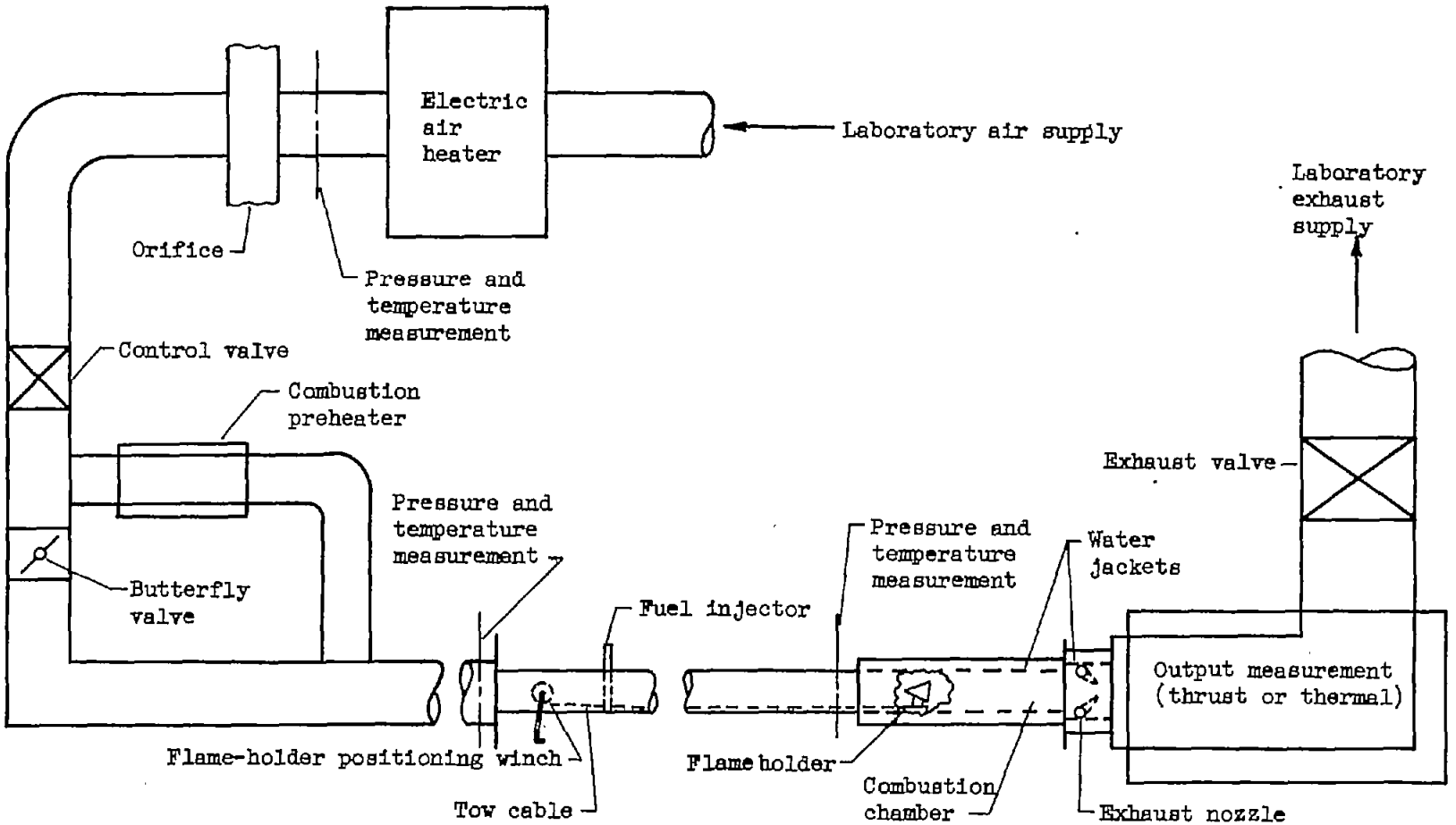

Figure 1. - Diagrammatic sketch of 6-inch afterburner installation.

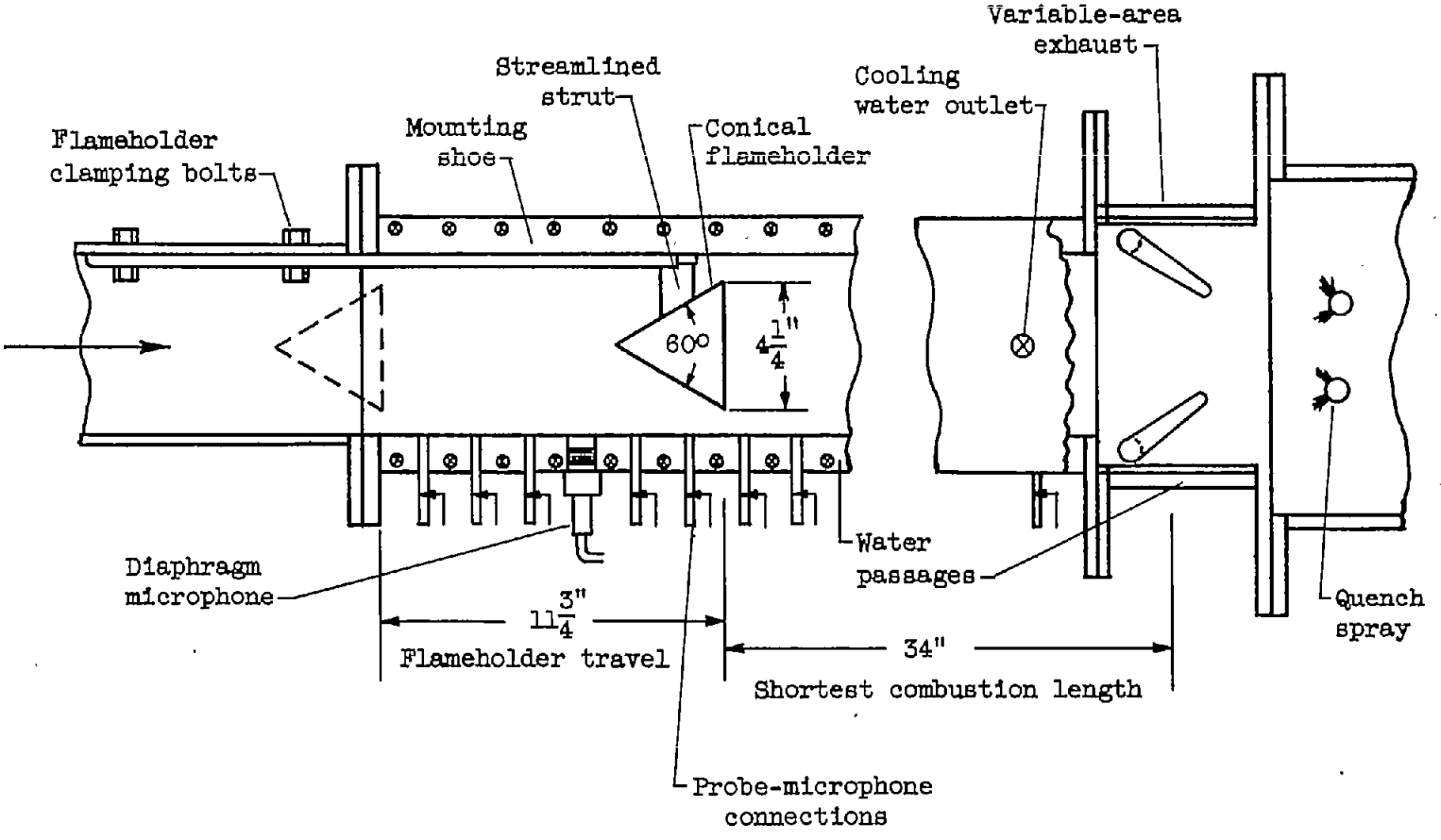

Figure 2. - Diagrammatic sketch of research combustor.

3070

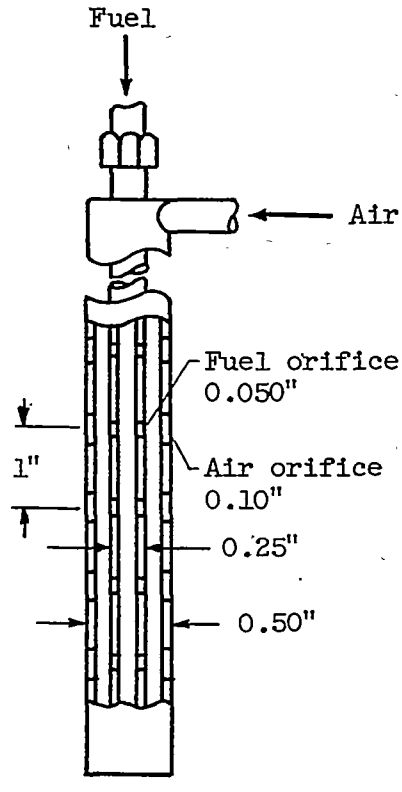

Figure 3. - Diagrammatic sketch of air-atomizing spray bar.

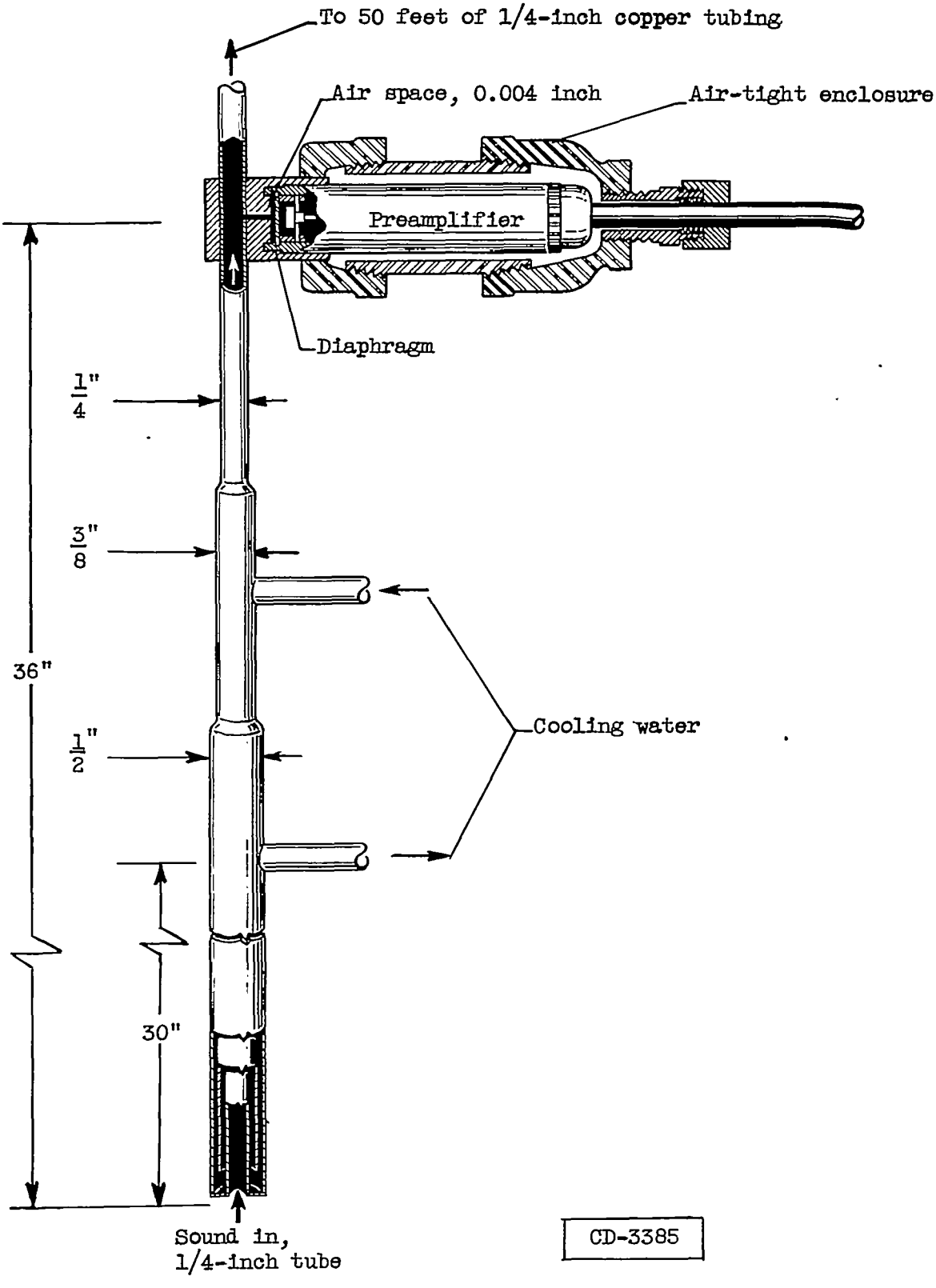

3070

Figure 4. - Sketch of "infinite" probe (not scaled).

3070

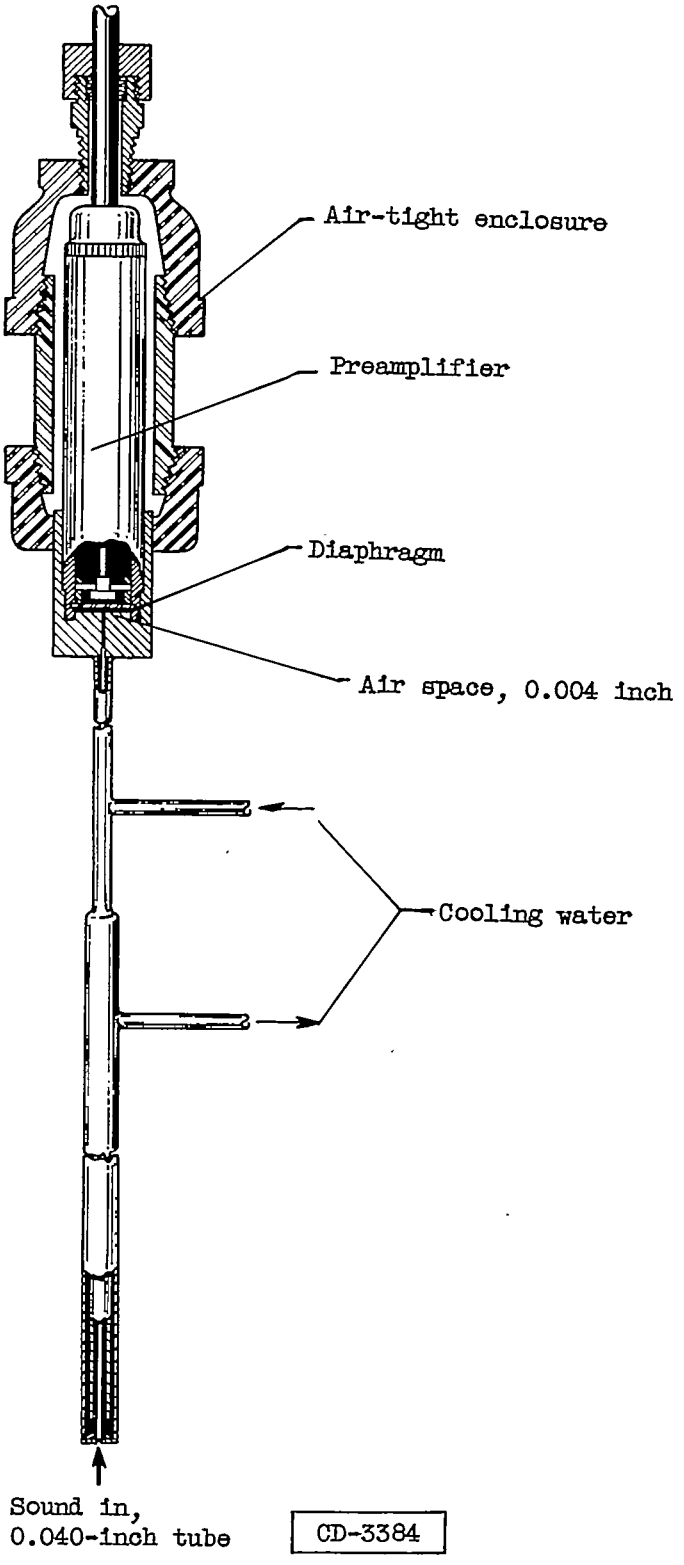

Figure 5. - Sketch of "phase" probe (not scaled).

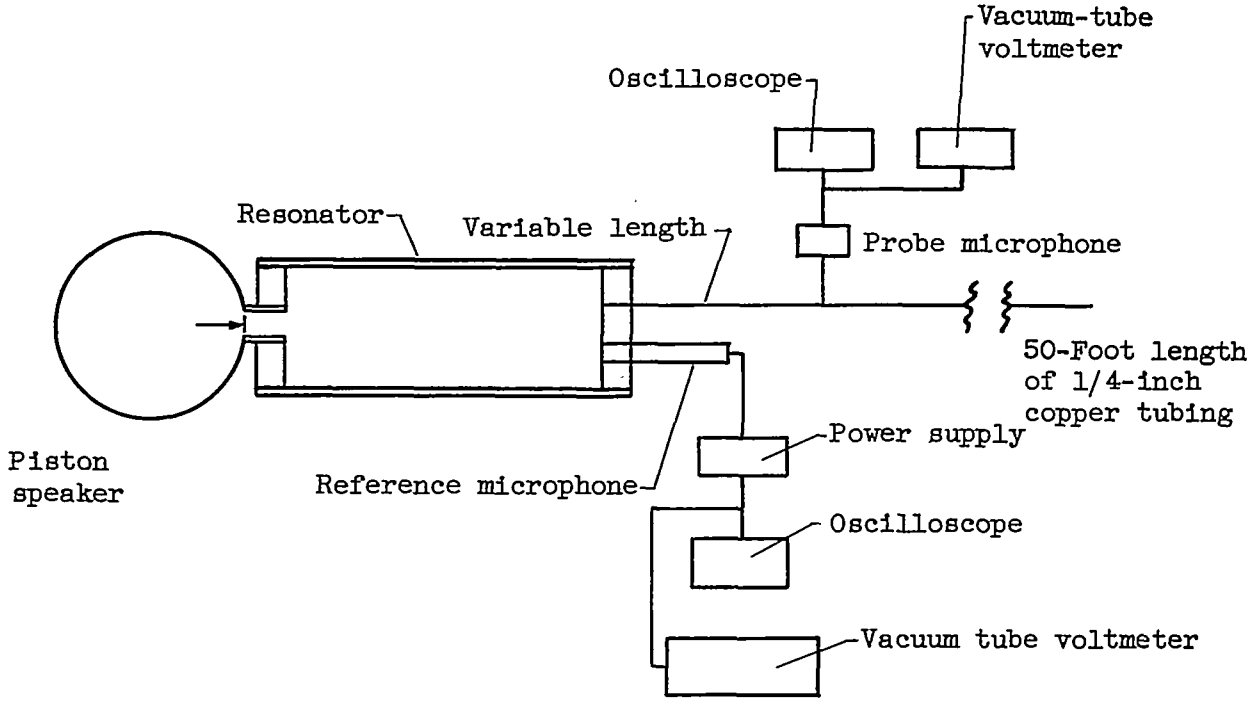

(a) Resonator for infinitesimals.

Figure 6. - Apparatus for measuring attenuation constants.

3070

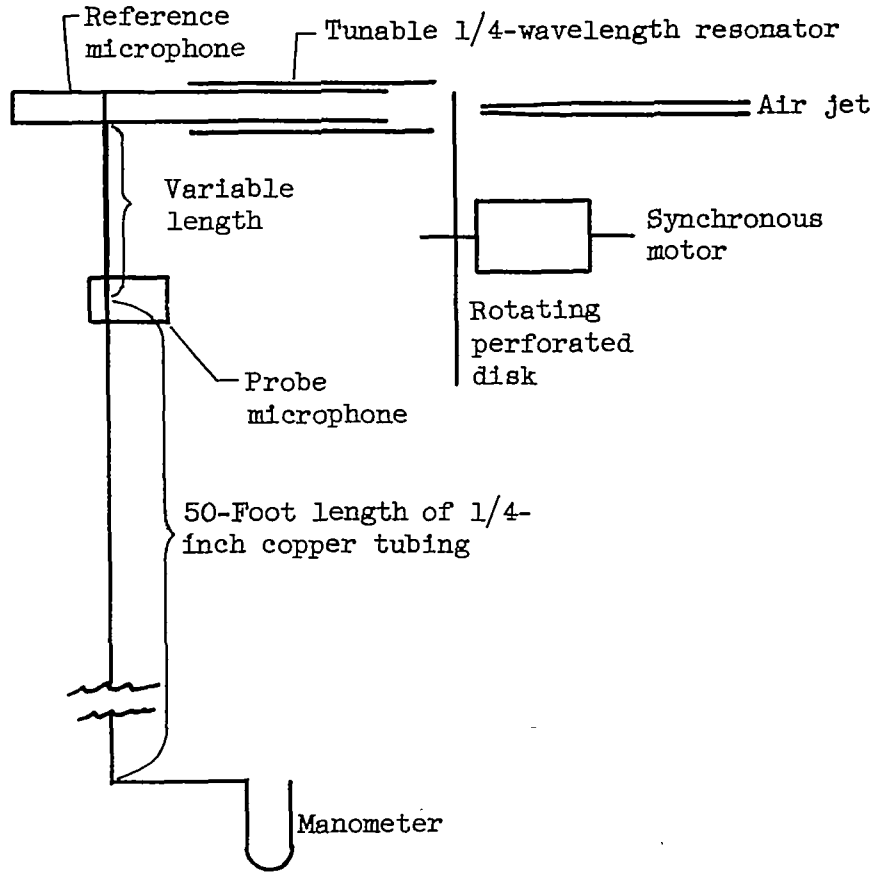

(b) Resonator for high amplitudes.

Figure 6. - Concluded. Apparatus for measuring attenuation constants.

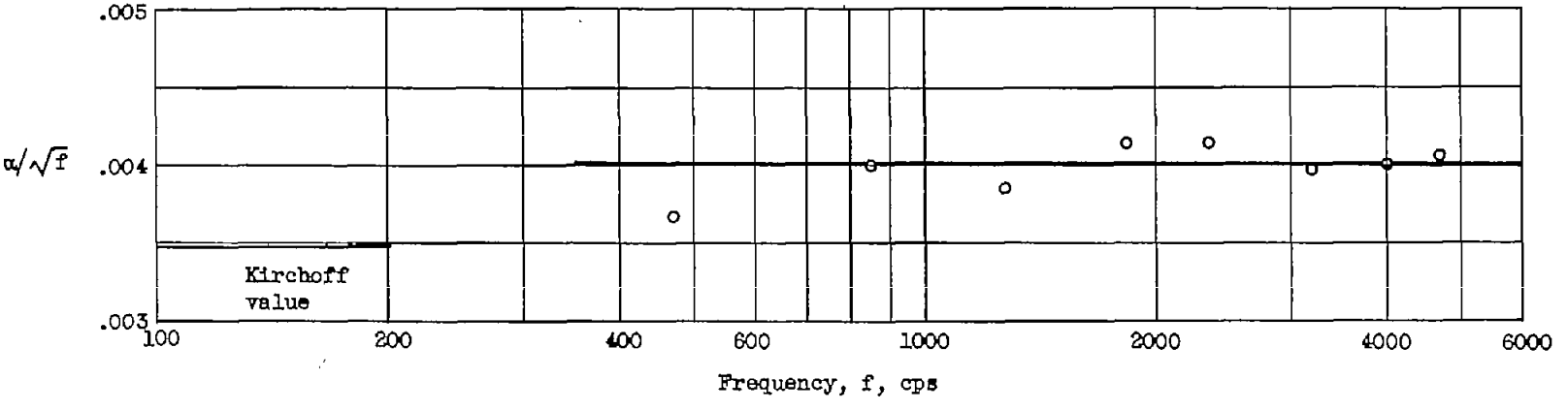

Figure 7. - Attenuation constant α for 1/4-inch-outside-diameter, 1/16-inch-wall copper tubing for low-amplitude sounds.

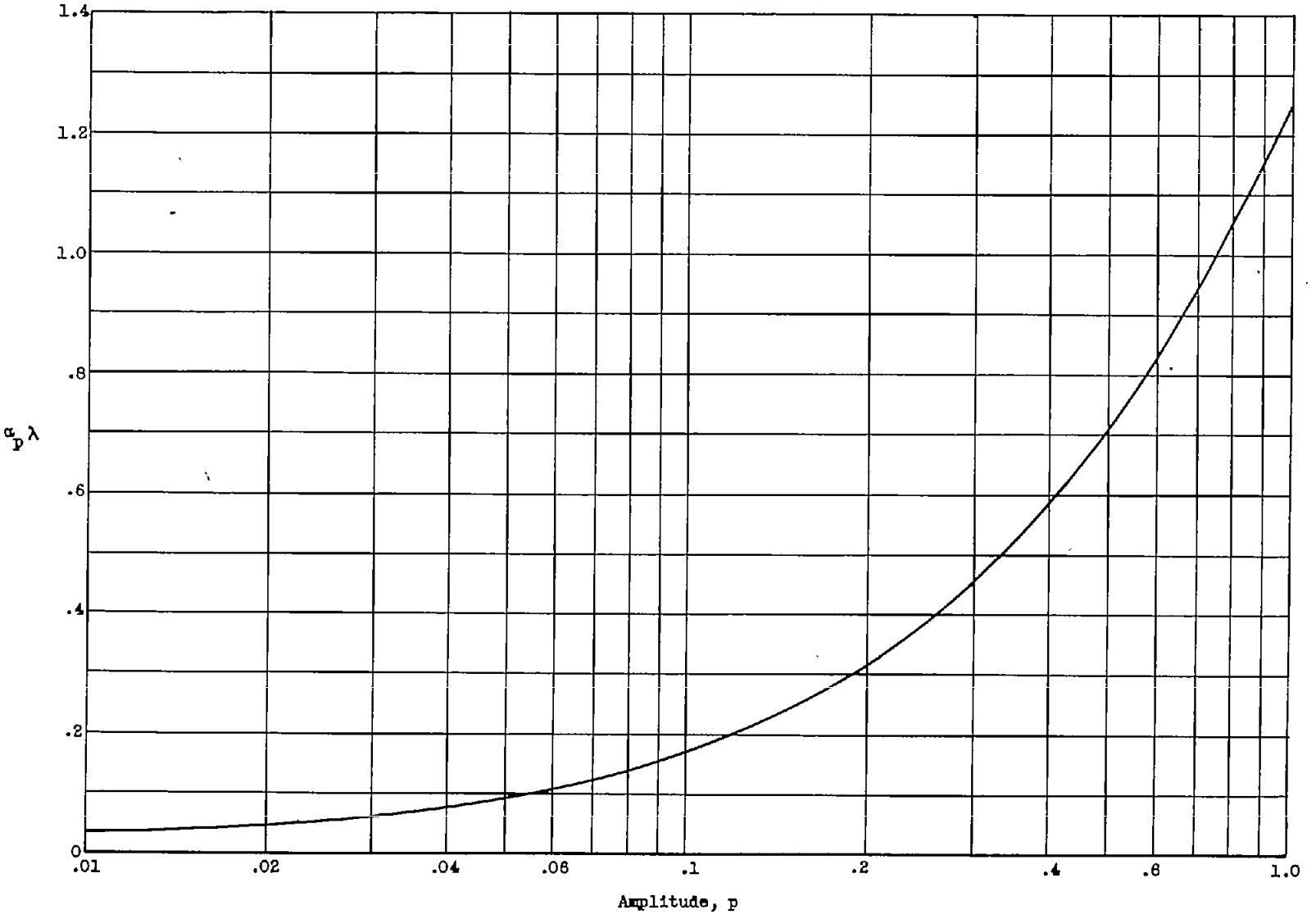

Figure 8. - Amplitude-dependent saw-tooth damping attenuation coefficient.

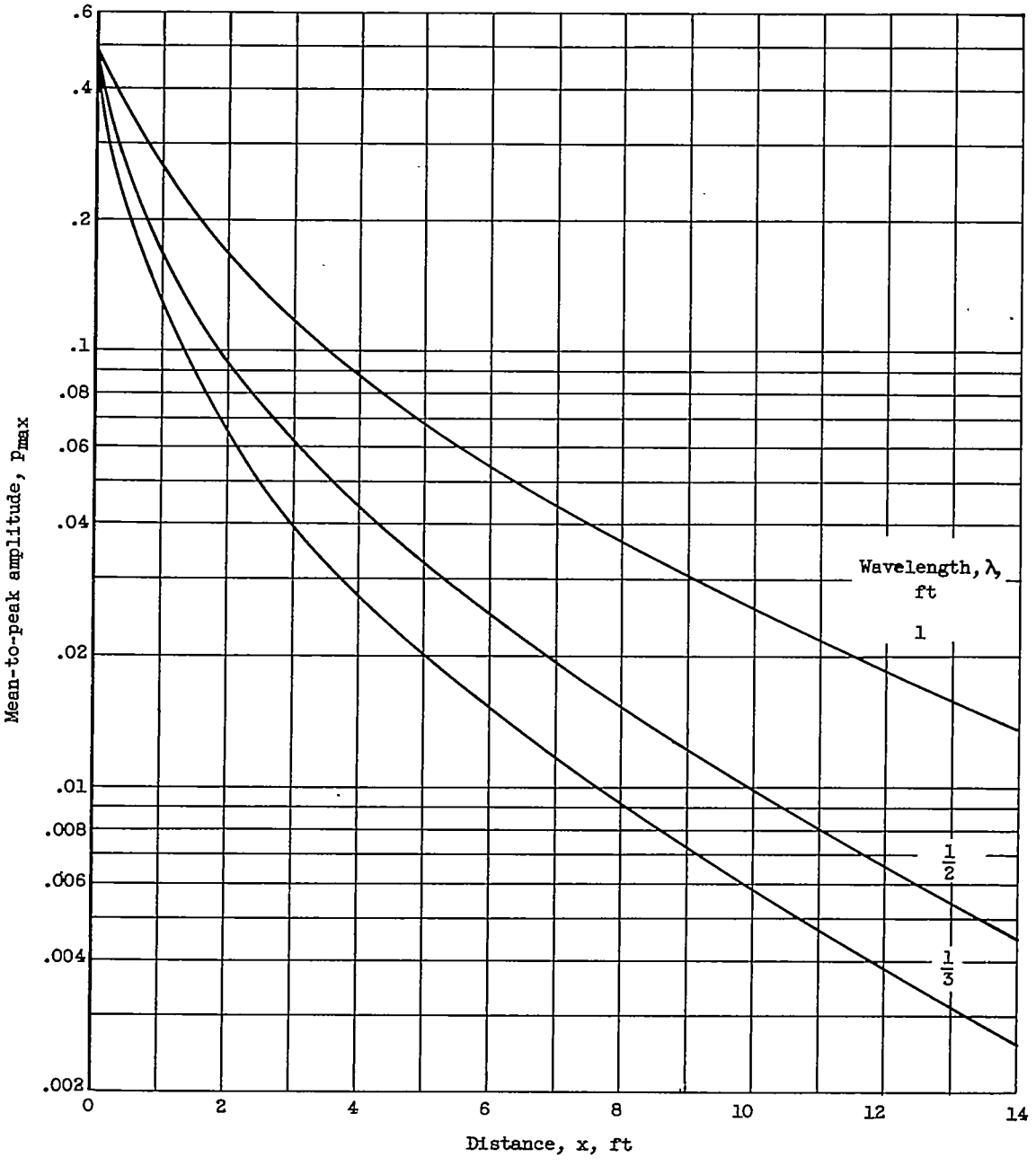

Figure 9. - Integrated theoretical attenuation curve for nonlinear and Kirchoff damping with $\alpha_k = \frac{0.126}{\sqrt{\lambda}}$.

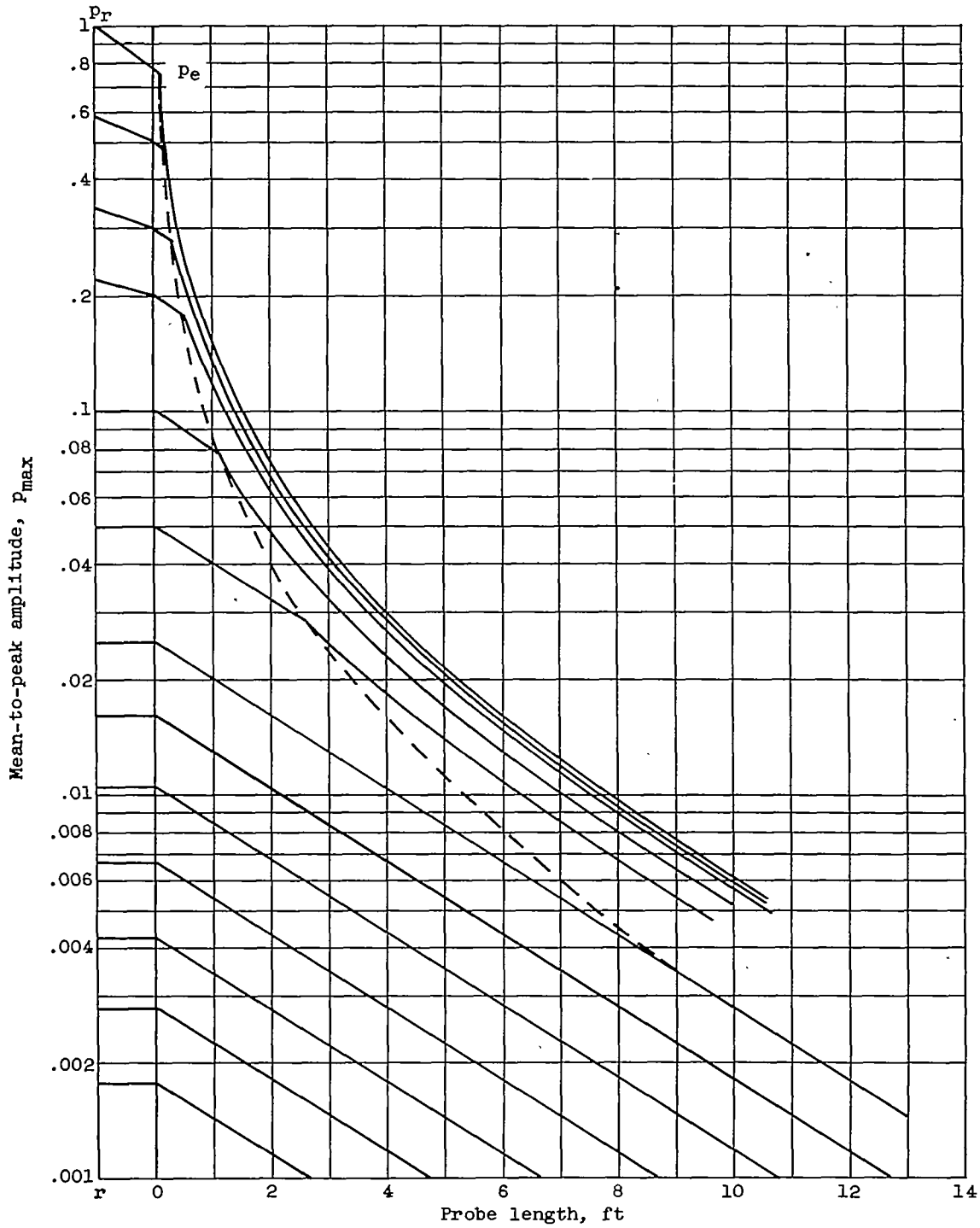

Figure 10. - Probe against reference amplitude incorporating end effects, length to become saw-toothed, and saw-tooth damping for 1/4-inch-outside-diameter, 1/32-inch-wall tubing. Frequency, 3000 cycles per second.

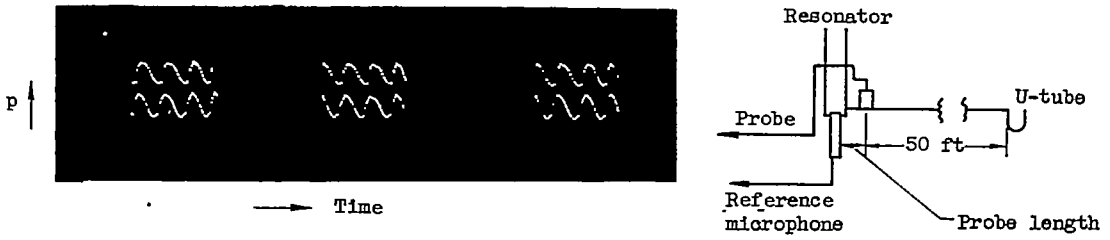

Probe length, 0.1 foot

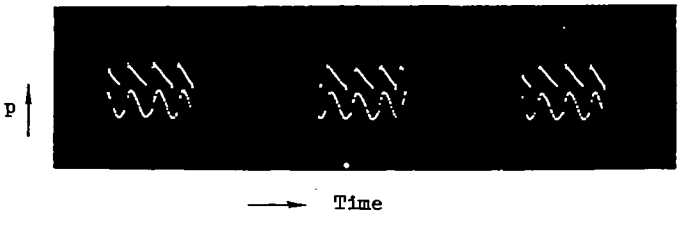

Probe length, 1.1 feet

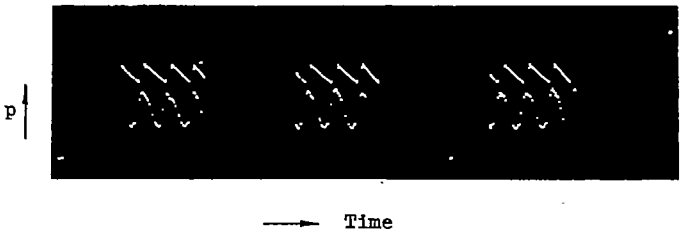

Probe length, 5.1 feet

Figure 11. - Wave form of "infinite" probe microphone and reference microphone for 1080 cycles per seconds. Pressure, 0.40 atmosphere.

3070

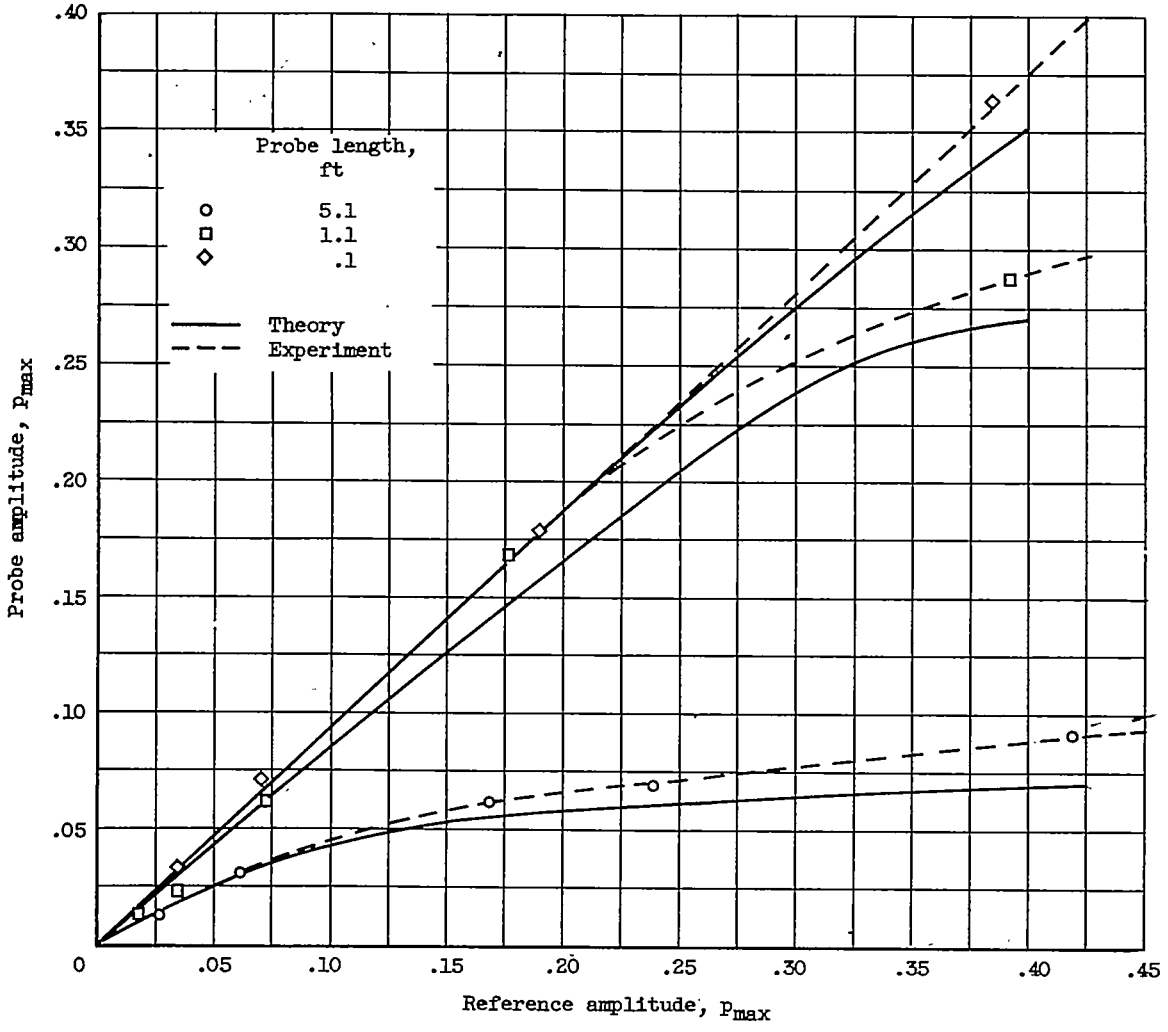

(a) Frequency, 1080 cycles per second.

Figure 12. - Probe-microphone calibration.

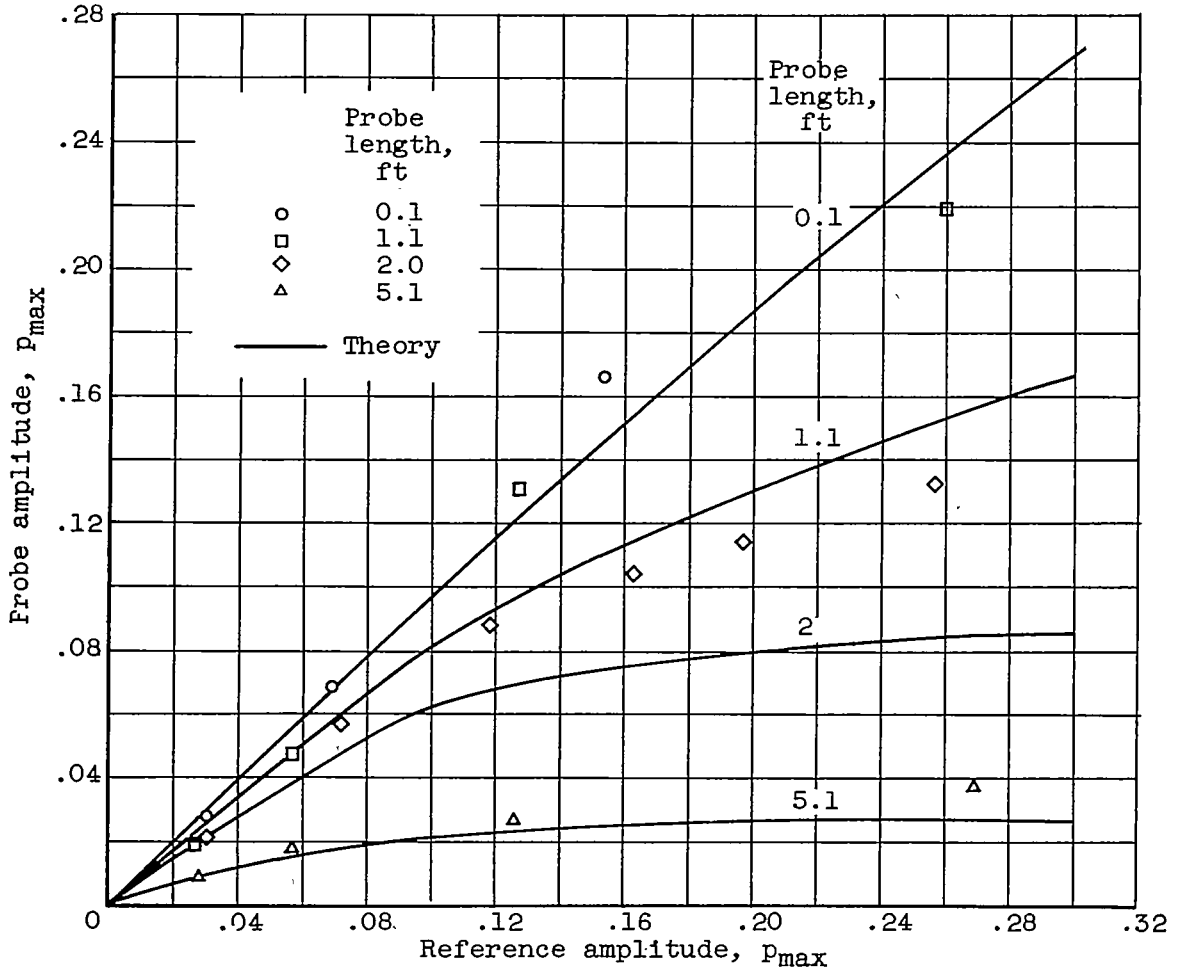

(b) Frequency, 2400 cycles per second.

Figure 12. - Continued. Probe-microphone calibration.

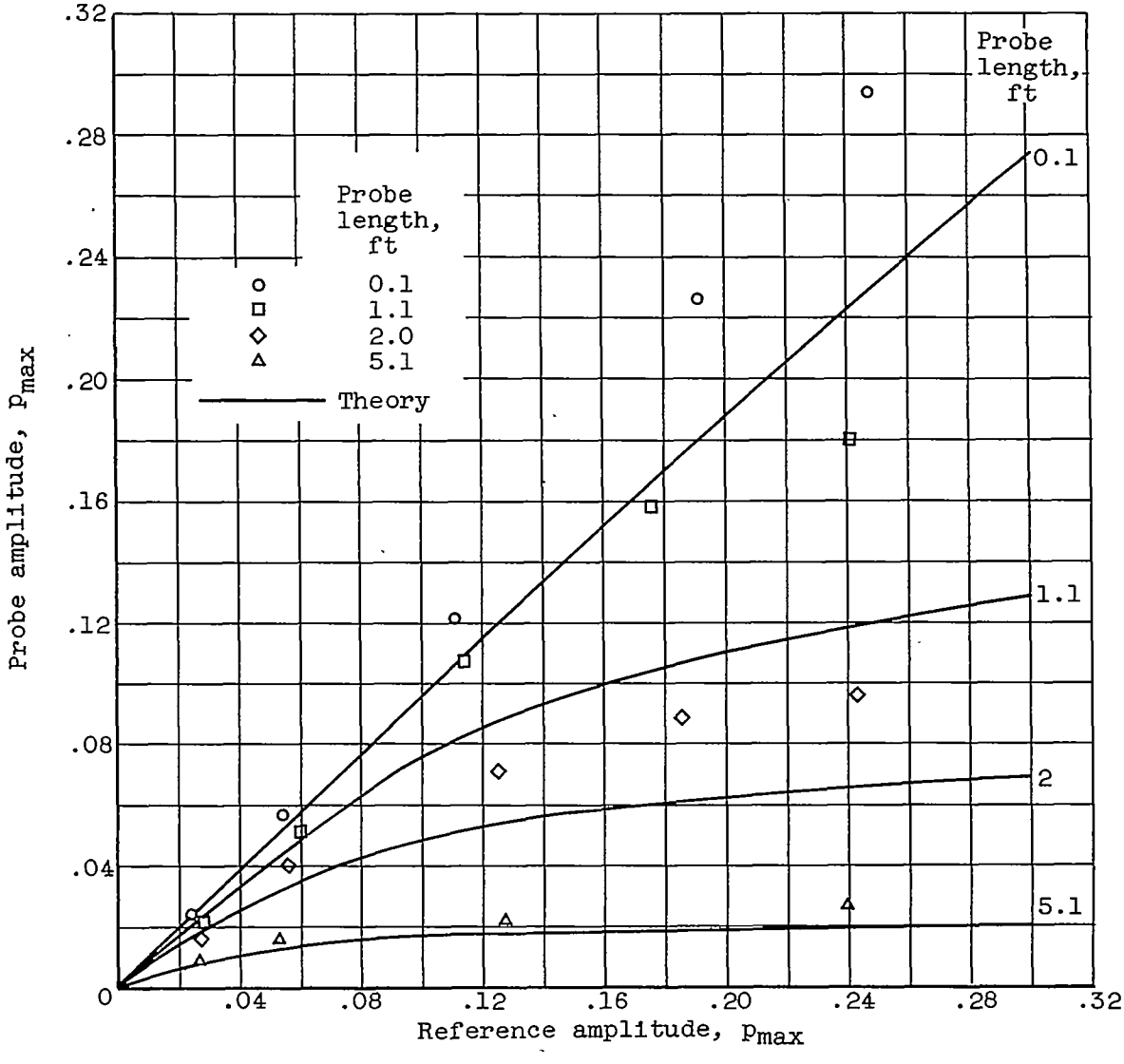

(c) Frequency, 3000 cycles per second.

Figure 12. - Concluded. Probe-microphone calibration.

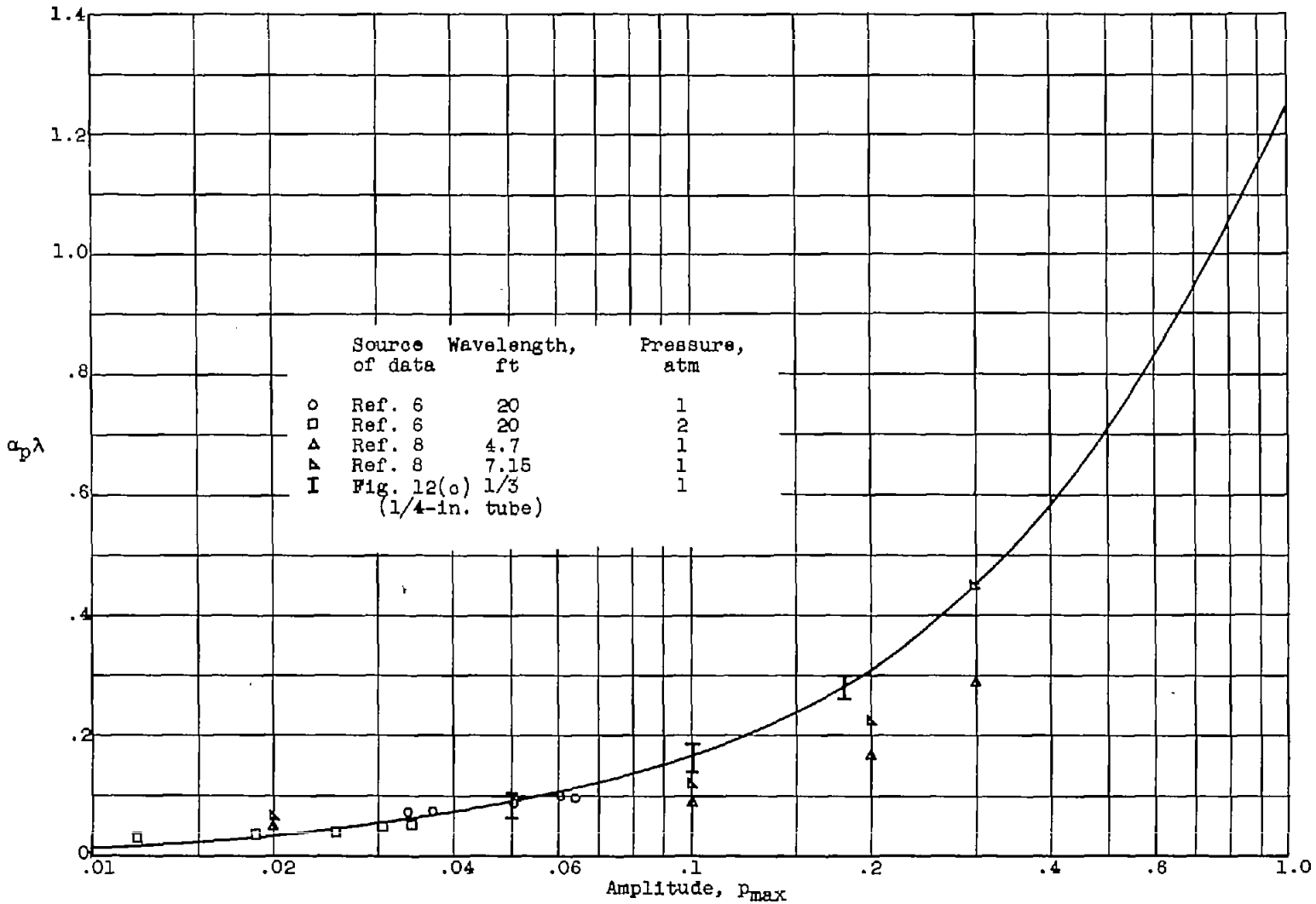

Figure 13. - Variation of amplitude-dependent damping coefficient $\alpha_p = \alpha - \alpha_k$ for saw-tooth waves with amplitude.

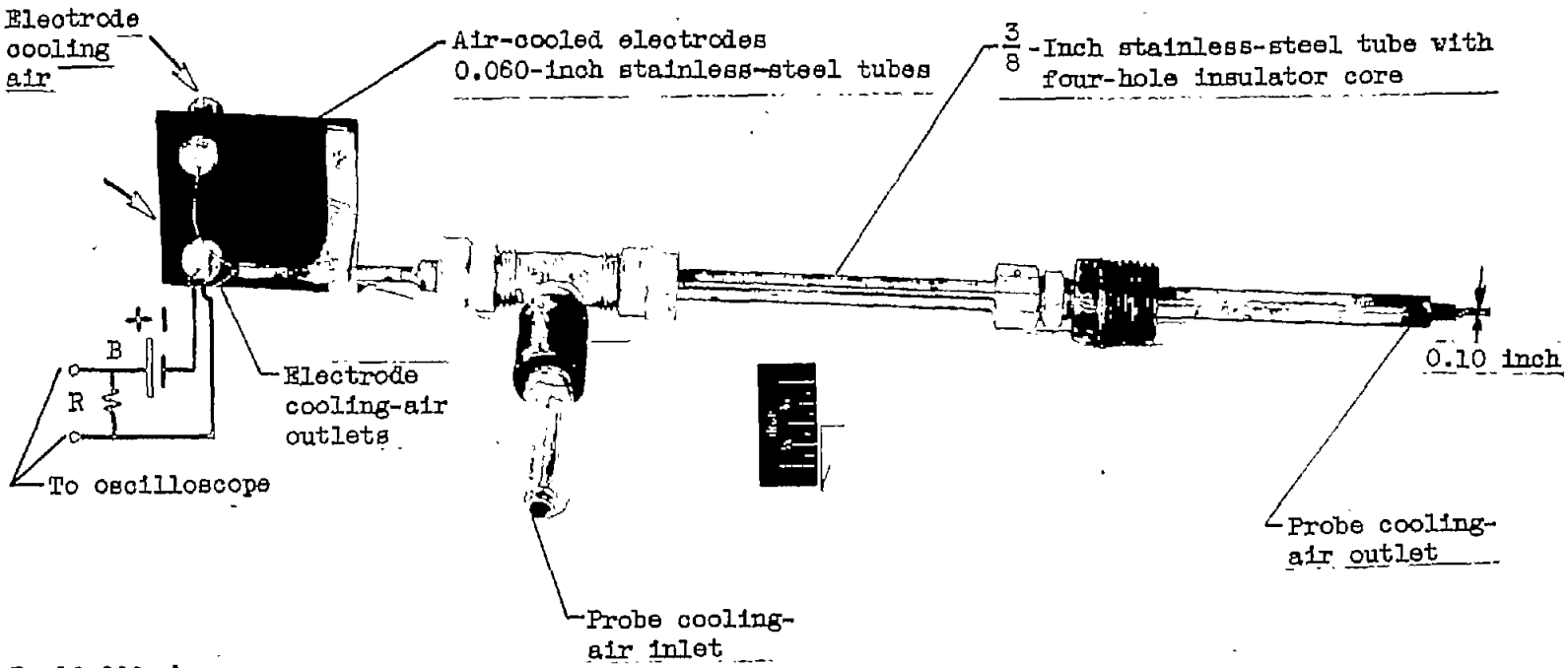

Figure 14. - Ionization gap.

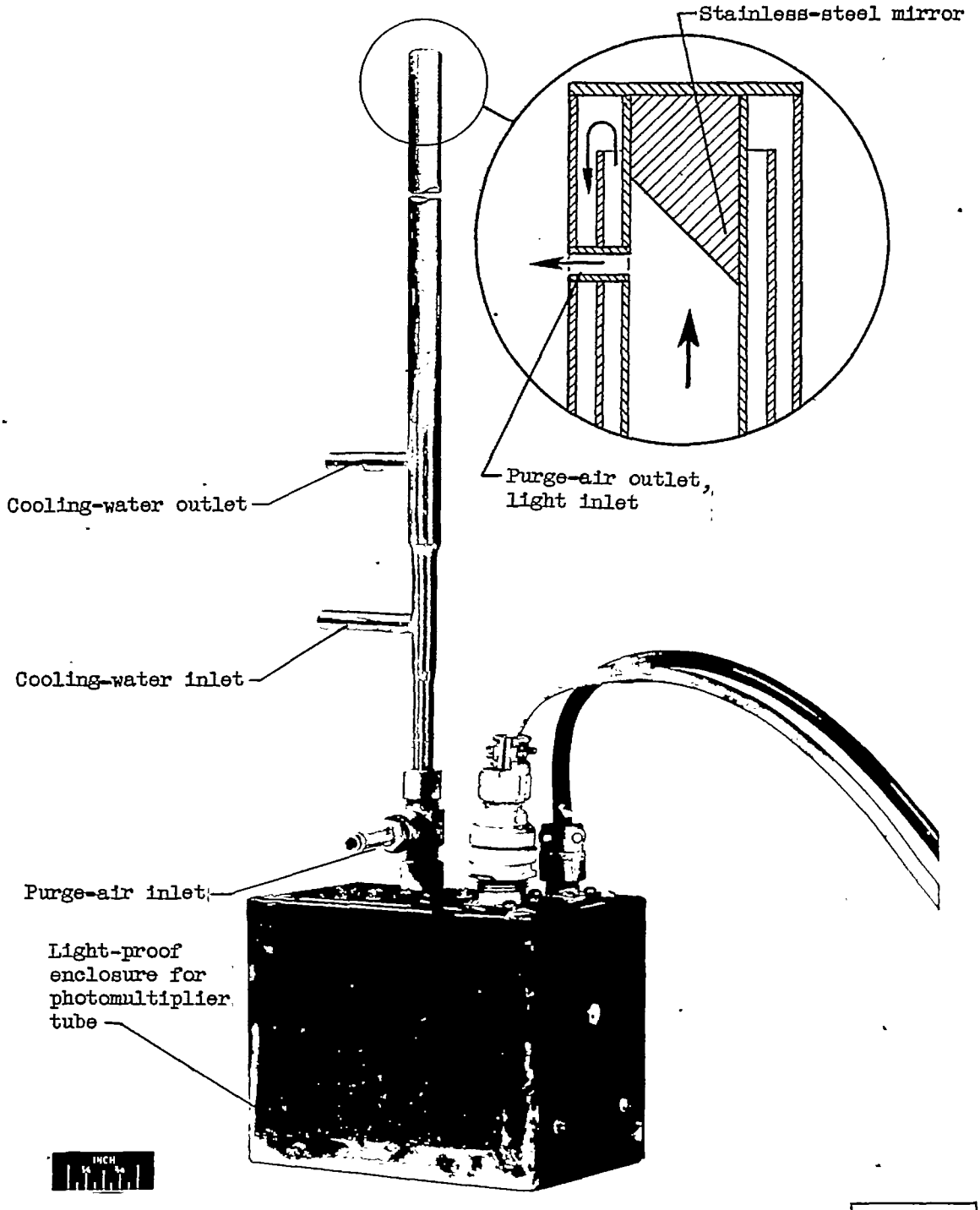

Figure 15. - Photocell probe.

C-33907

3070

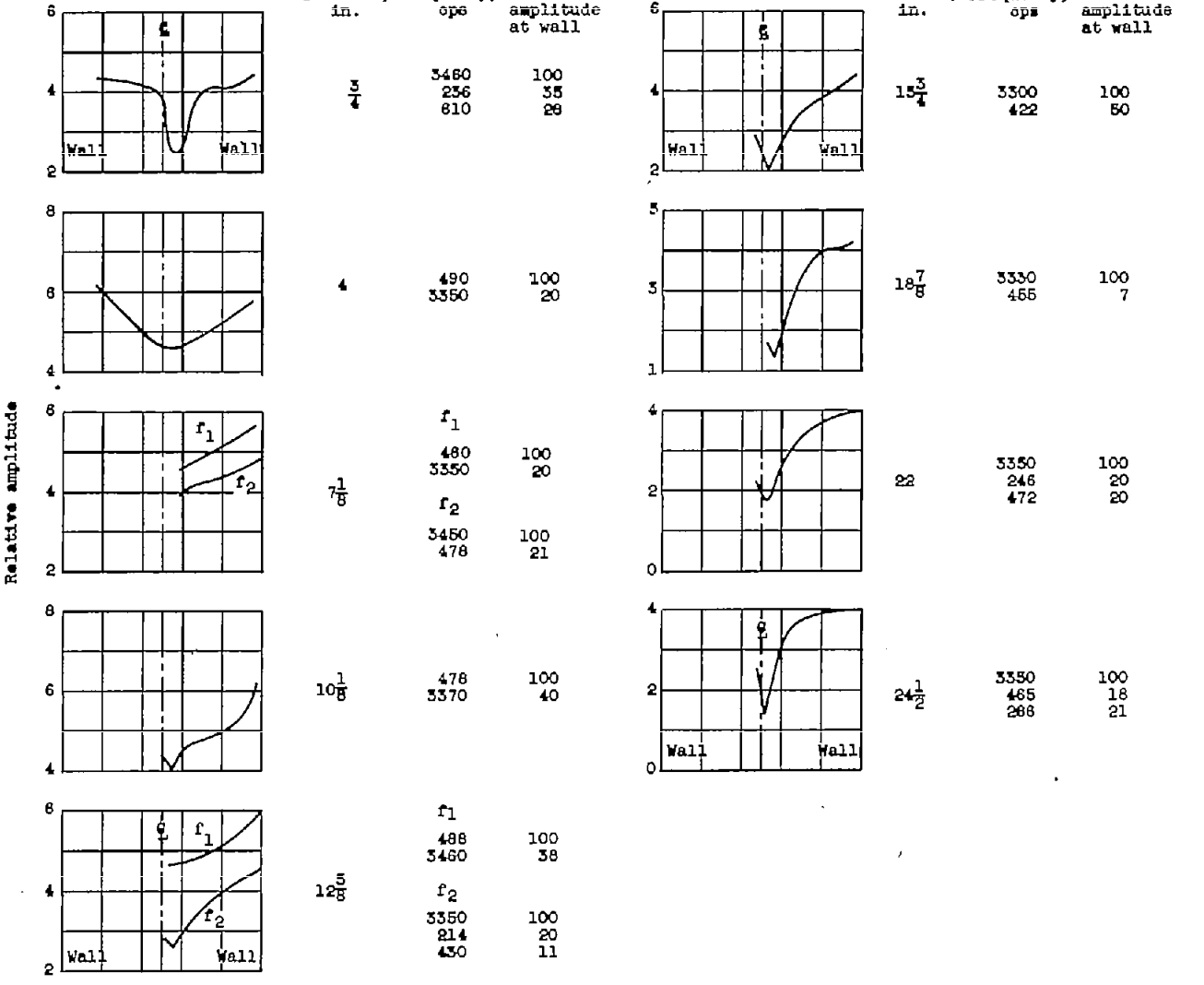

Flame-holder distance, in.	Spectral distribution: Frequency, cps	Relative amplitude at wall
$\frac{3}{4}$	3460	100
	256	35
	610	28
4	490	100
	3350	20
$7\frac{1}{8}$	f_1	
	480	100
	3350	20
	f_2	
	3450	100
	478	21
$10\frac{1}{8}$	478	100
	3370	40
$12\frac{5}{8}$	f_1	
	488	100
	3460	38
	f_2	
	3350	100
	214	20
	430	11
$15\frac{3}{4}$	3300	100
	422	50
$18\frac{7}{8}$	3330	100
	455	7
22	3350	100
	246	20
	472	20
$24\frac{1}{2}$	3350	100
	465	18
	288	21

Figure 16. - Amplitude profiles across combustor for seven flameholder positions.

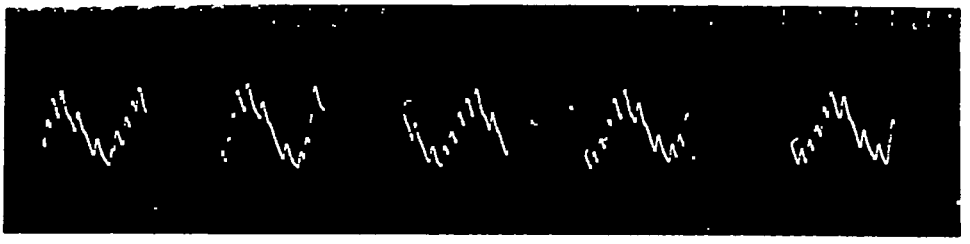

(a) Screech plus longitudinal resonance.

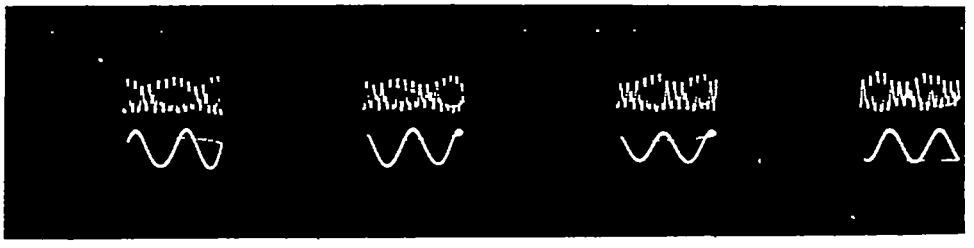

(b) Simultaneous trace of filtered major components in figure 17(a) showing modulation of screech by low-frequency note.

Figure 17. - Wave forms of screech and longitudinal resonance.

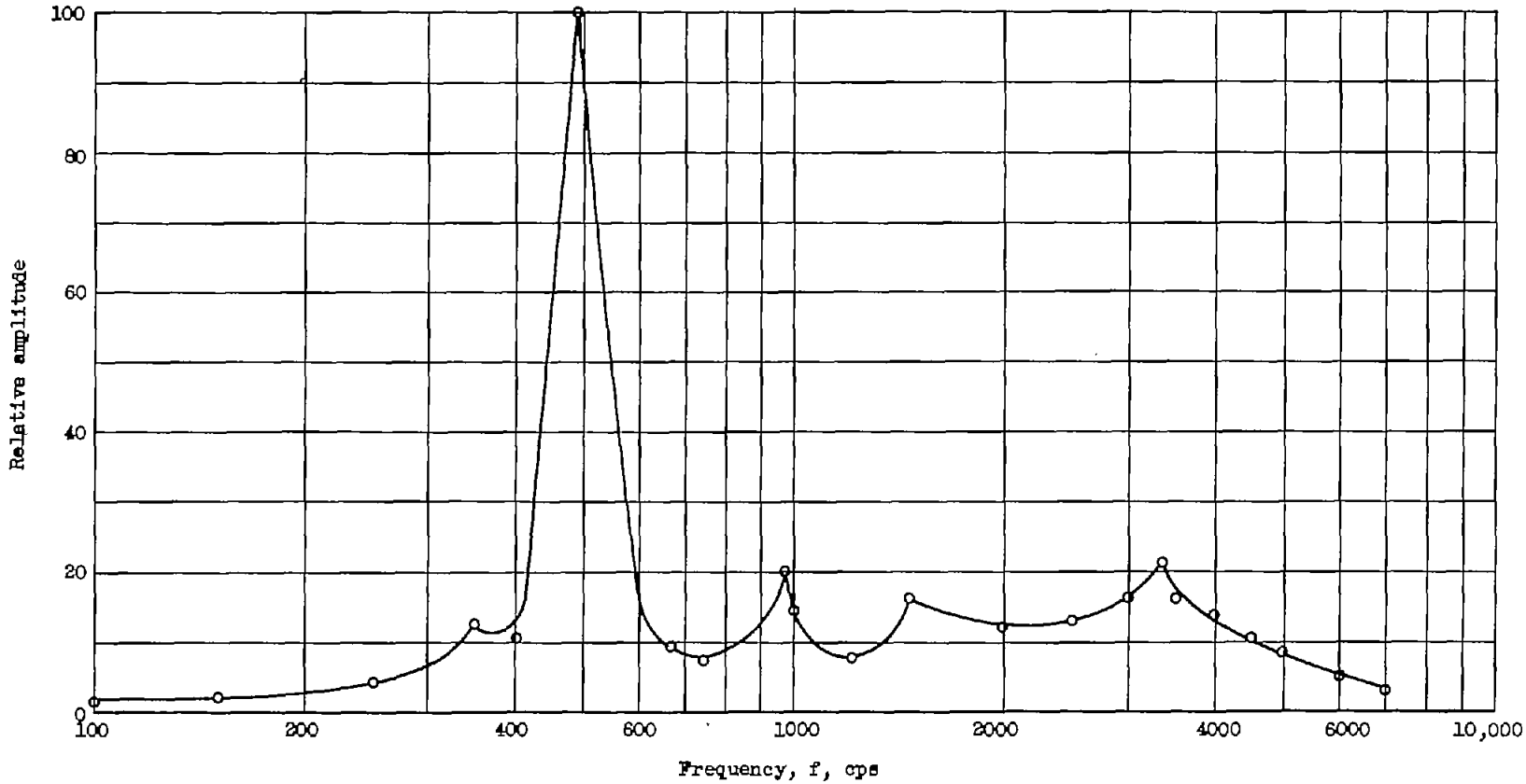

(a) Predominantly low-frequency spectrum; measured 4 inches downstream.

Figure 18. - Examples of spectra at wall downstream of flameholders.

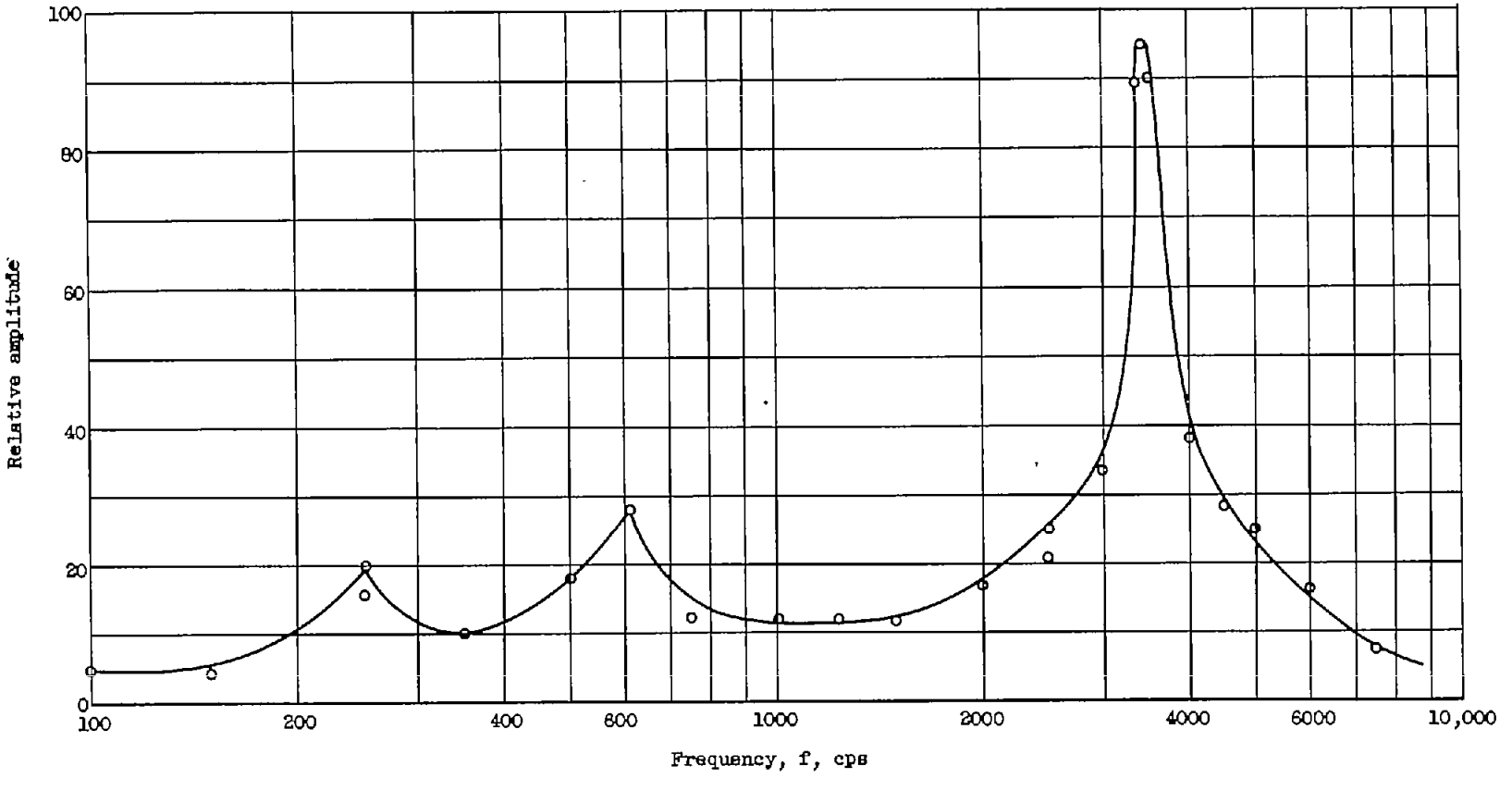

(b) Predominantly high-frequency spectrum; measured 3/4 inch downstream.

Figure 18. - Concluded. Examples of spectra at wall downstream of flameholders.

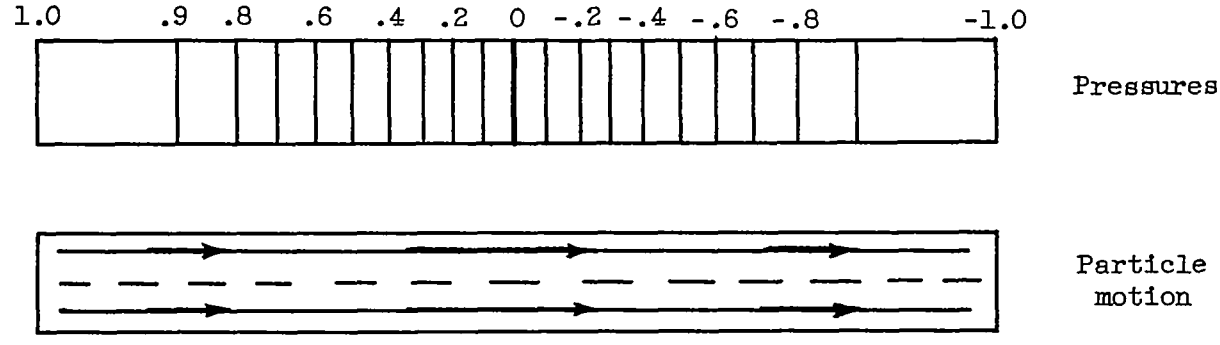

(a) First longitudinal mode.

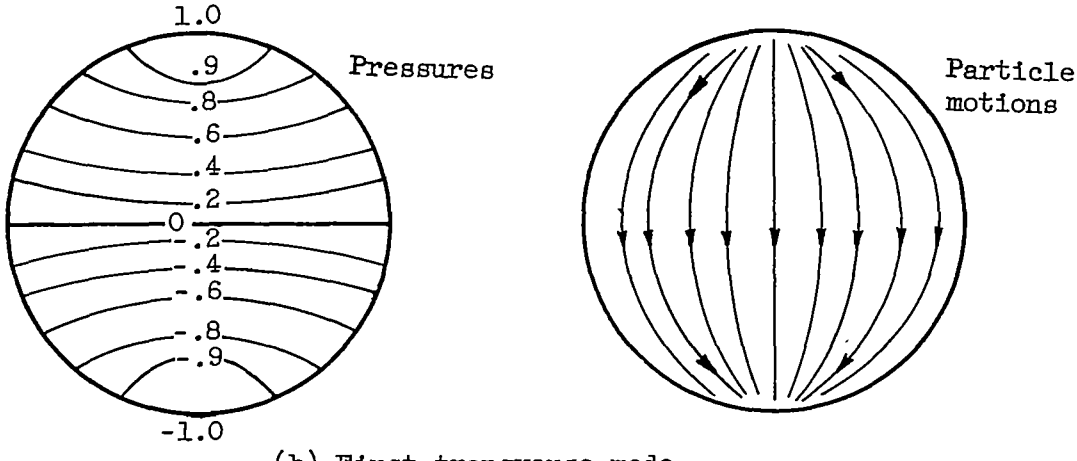

(b) First transverse mode.

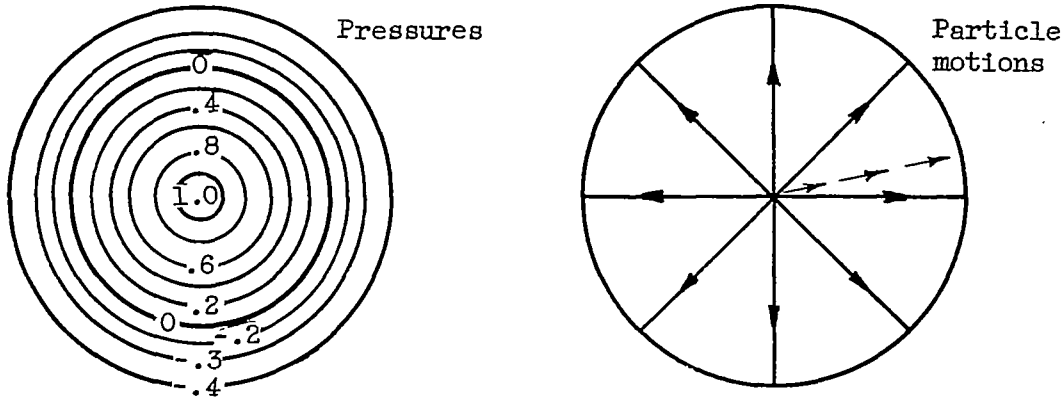

(c) First radial mode.

Figure 19. - Pressure contours and particle motions for fundamental modes of cylindrical duct.

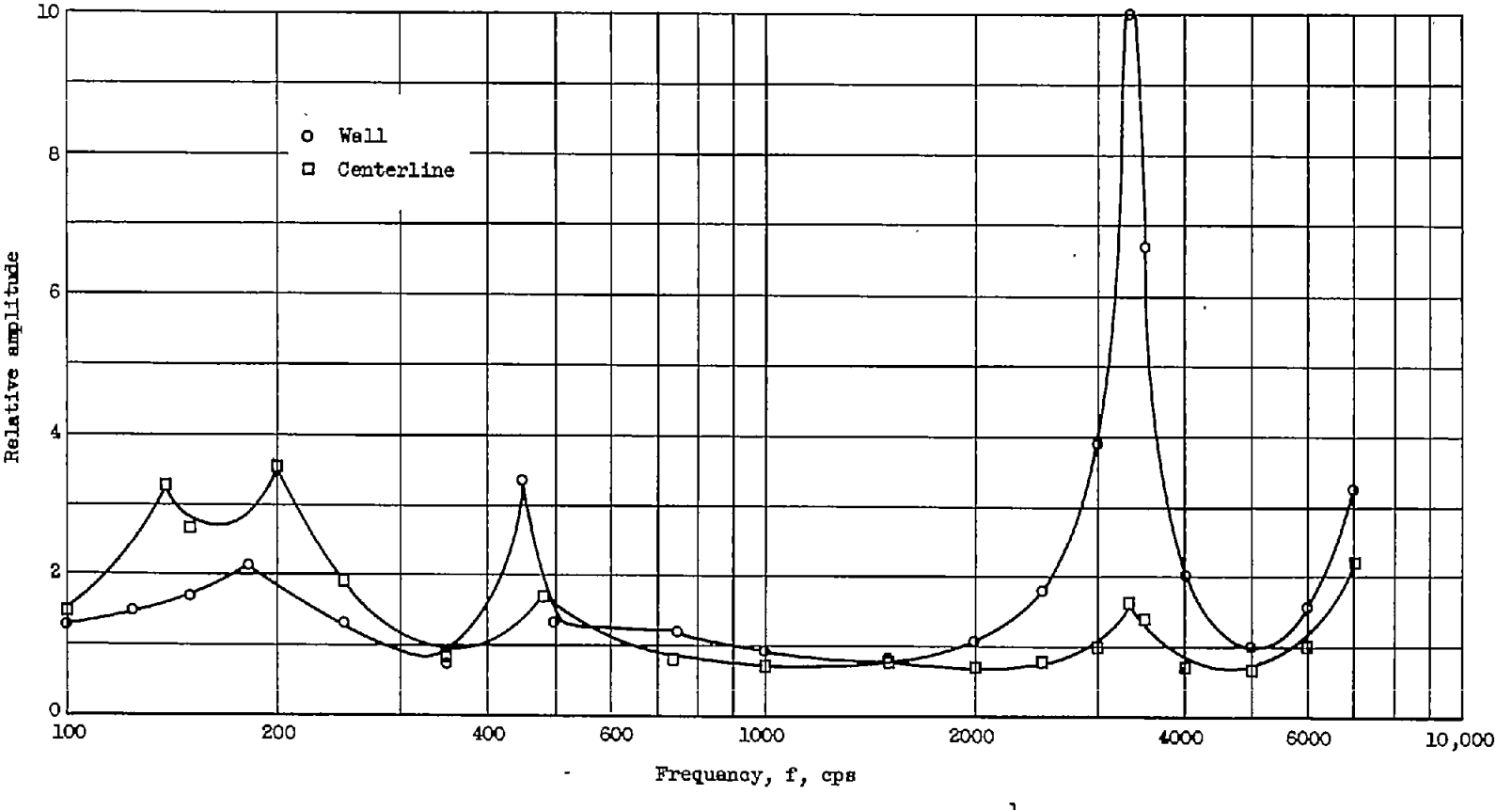

Figure 20. - Comparison of sound spectra at combustor wall and at centerline 24½ inches downstream of flameholder.

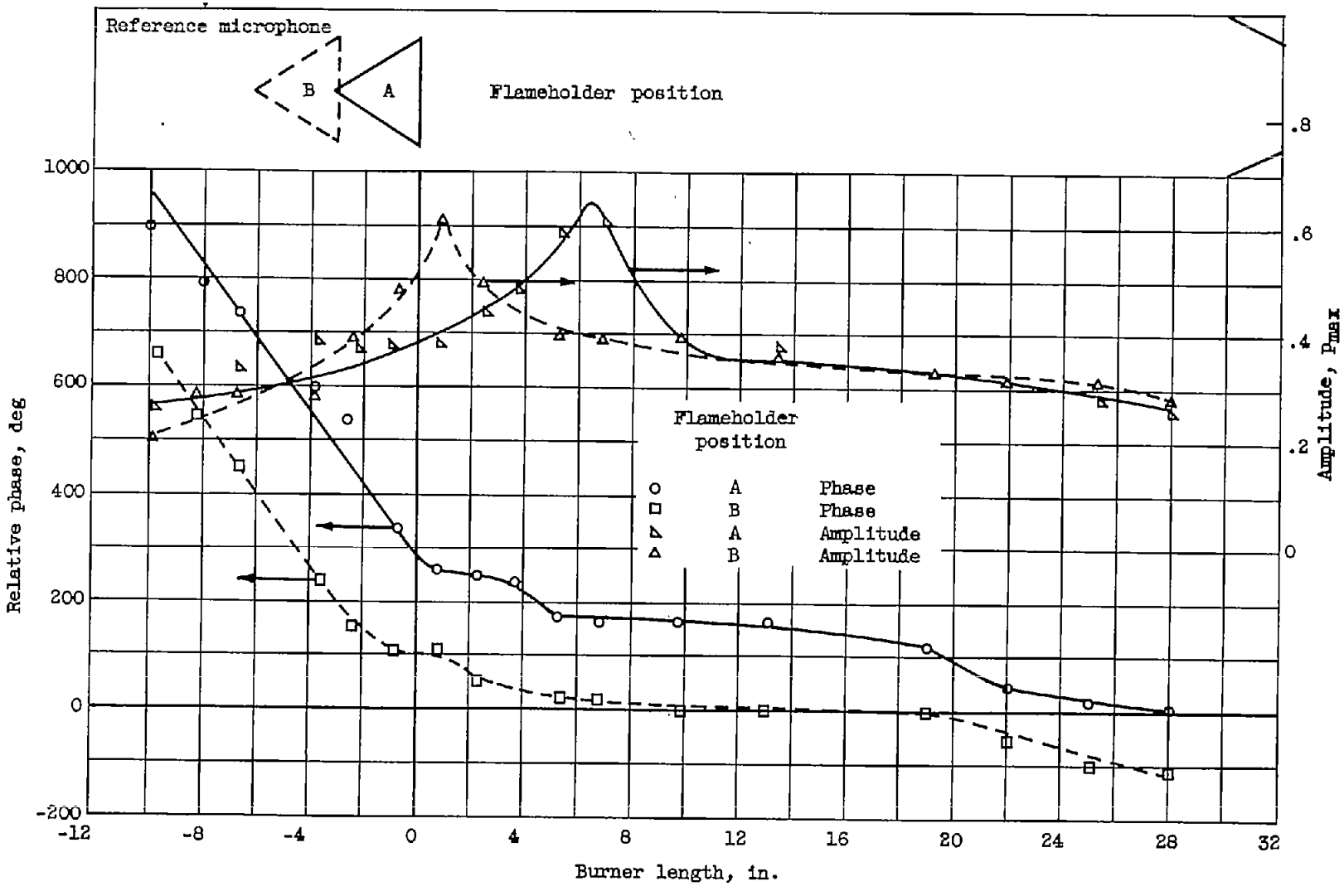

Figure 21. - Amplitude and phase distributions for two flameholder positions.

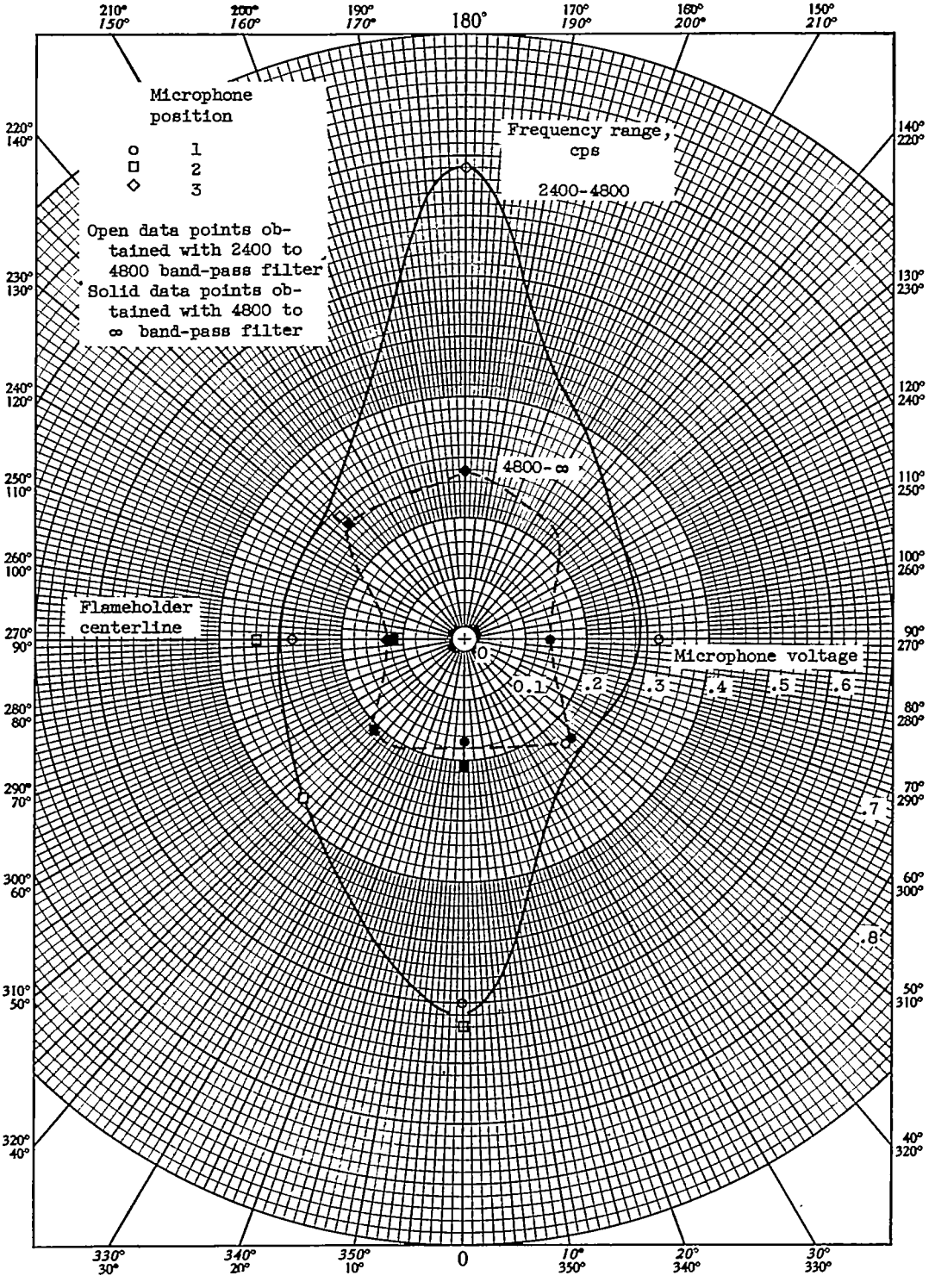

Figure 22. - Microphone voltages about circumference of screeching combustor $1\frac{1}{2}$ inches downstream of V-gutter.

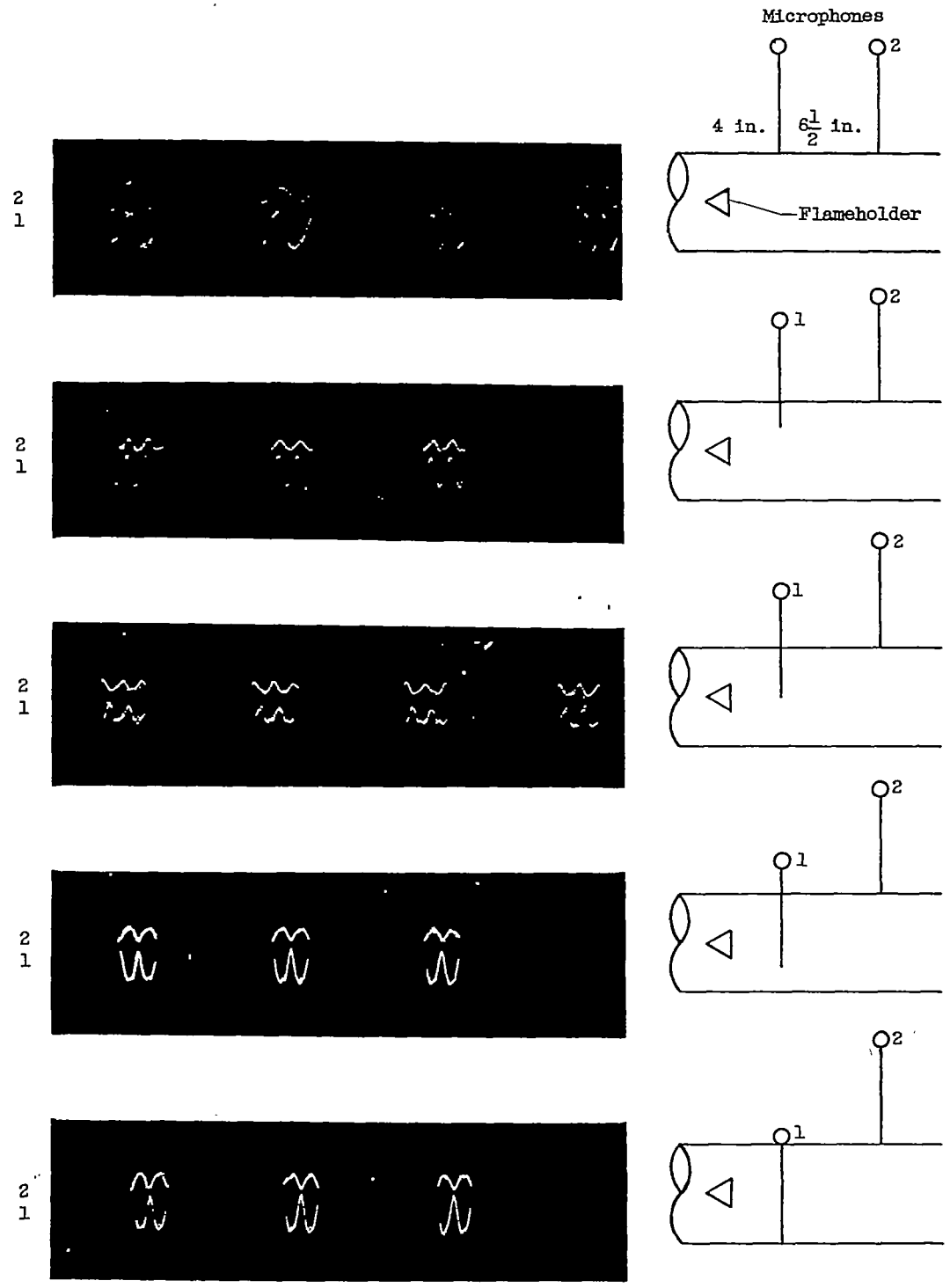

Figure 23. - Pressure signal from two phase probe microphones showing phase shift along a diameter.

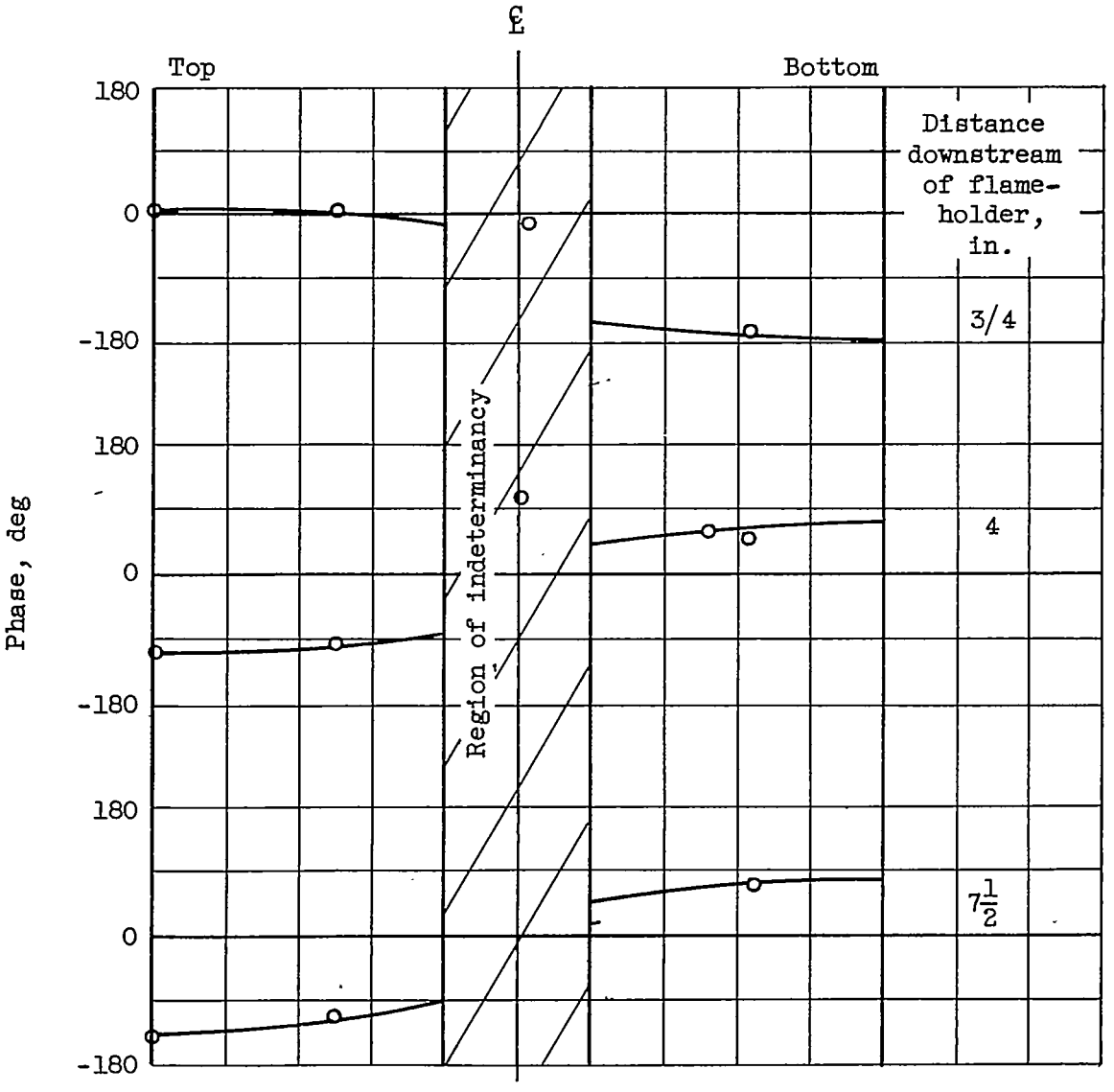

Figure 24. - Phase of pressure signal relative to signal at top of combustor 3/4 inch downstream of flameholder for three flameholder positions.

3070

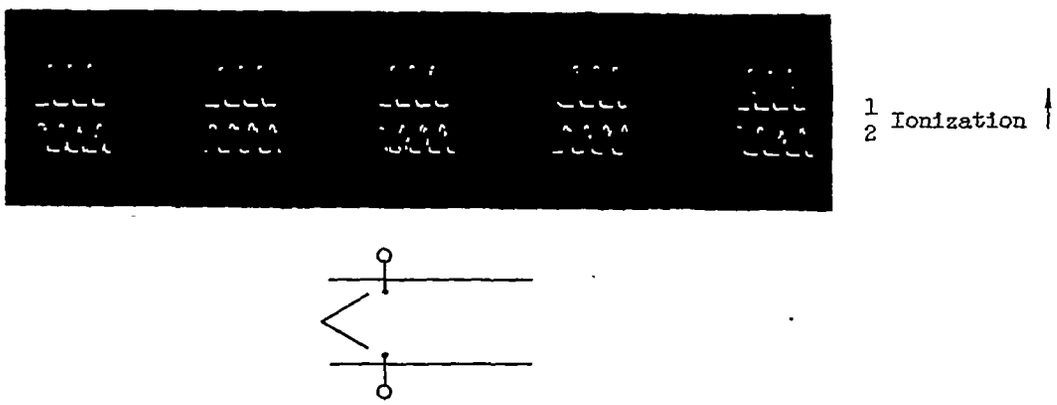

(a) Ionization traces at top and bottom of combustor 3/4 inch from wall.

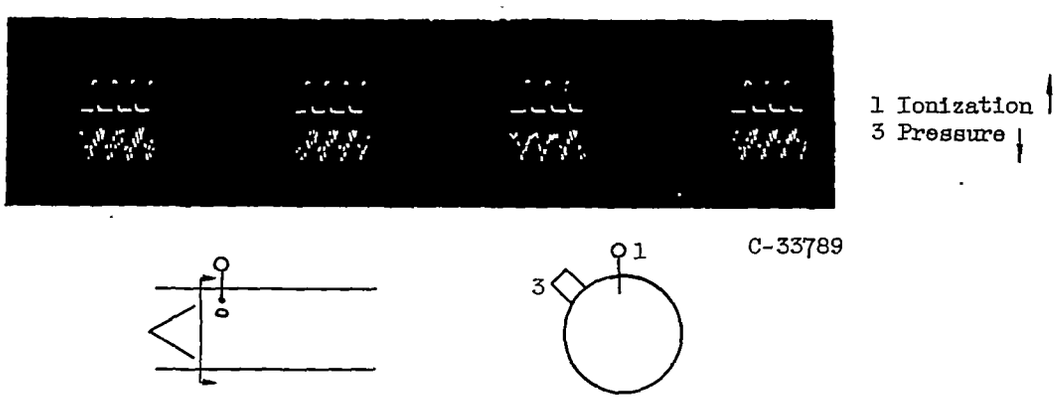

(b) Ionization and pressure traces at top and 60° from top of combustor.

Figure 25. - Ionization and pressure traces 3/4 inch downstream of flameholder.

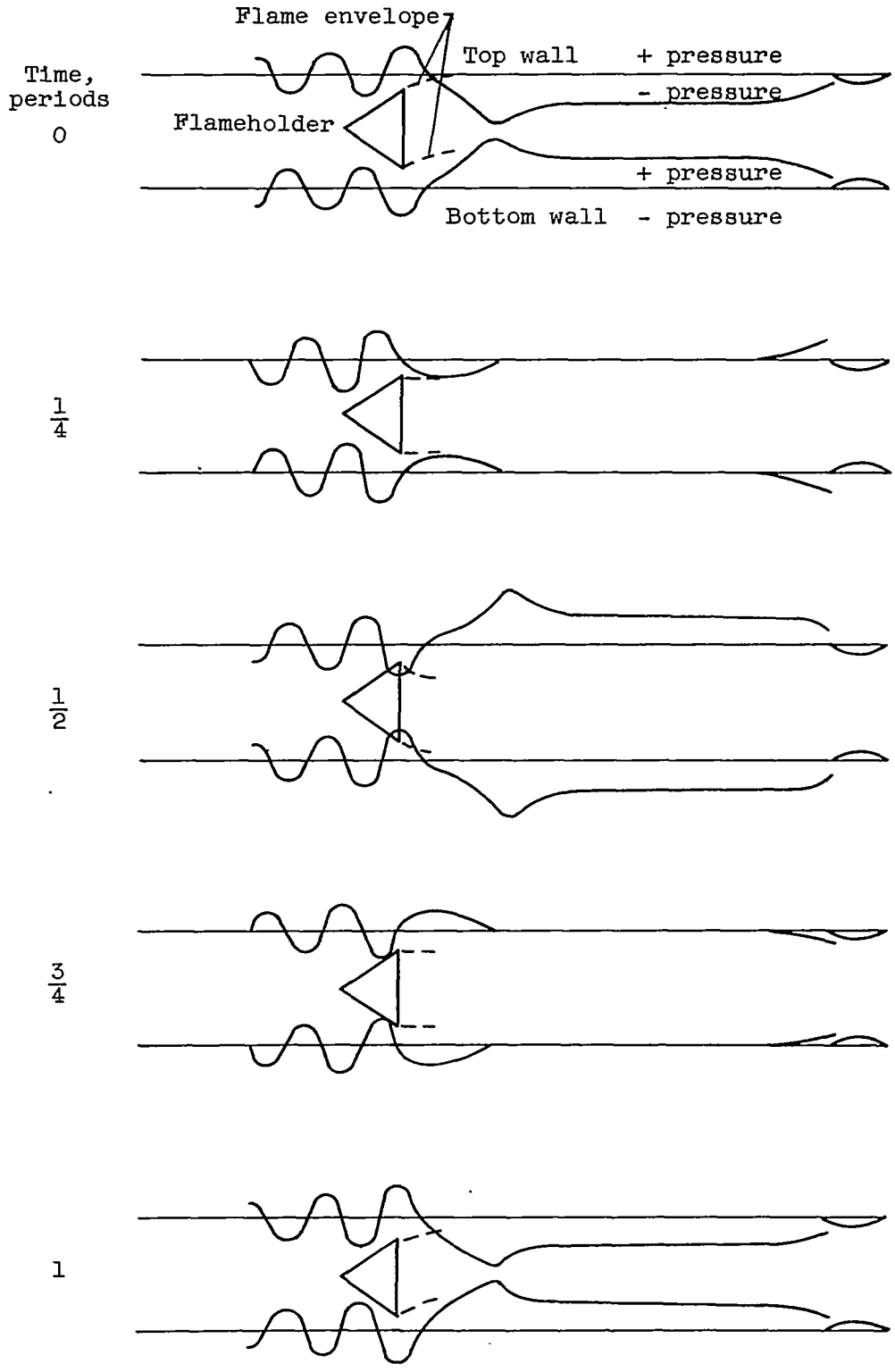

Figure 26. - Reconstruction of pressure and flame-displacement sequence.

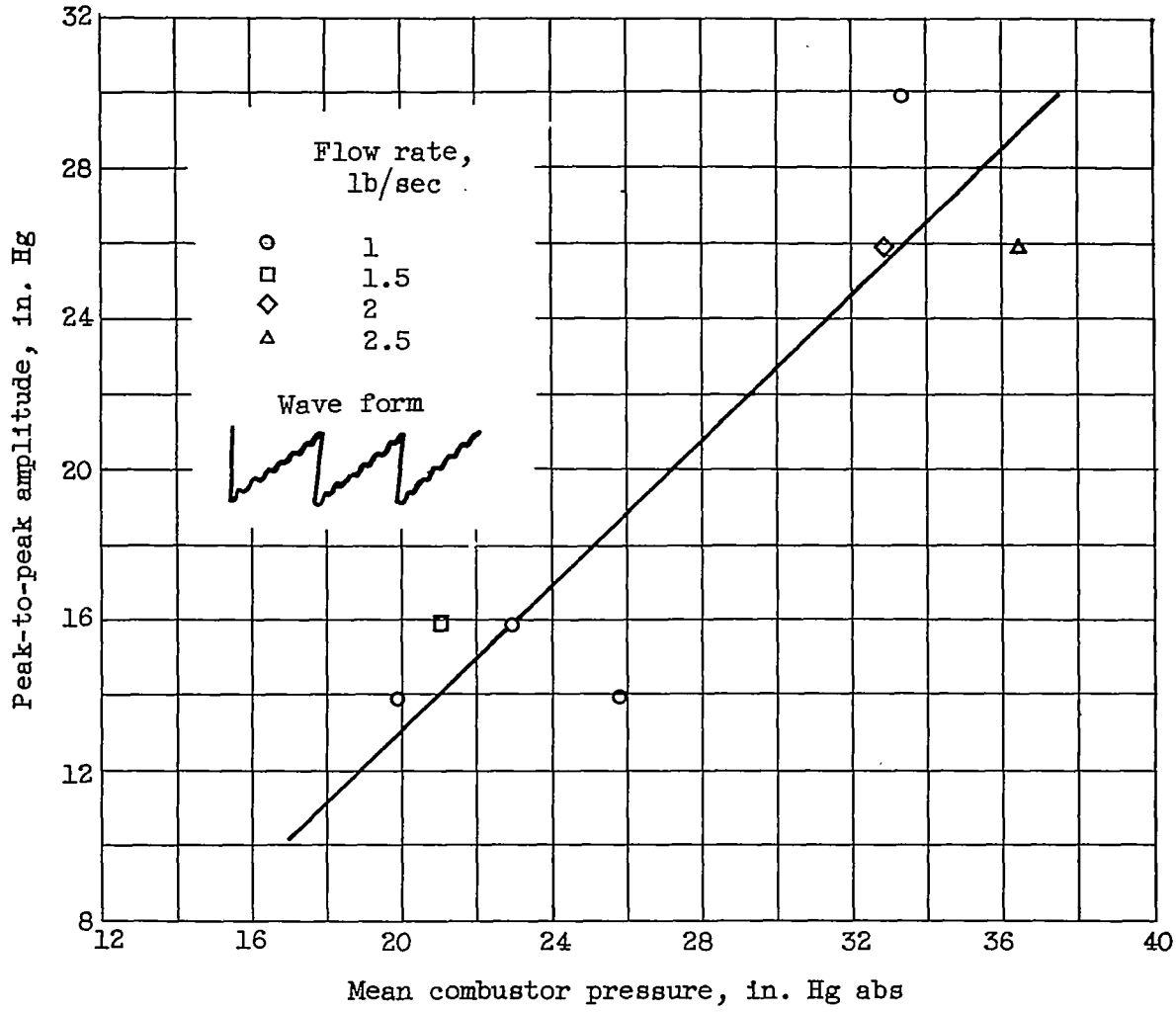

Figure 27. - Peak-to-peak screech amplitudes measured $5\frac{1}{4}$ inches upstream of flameholder for four different flow rates.

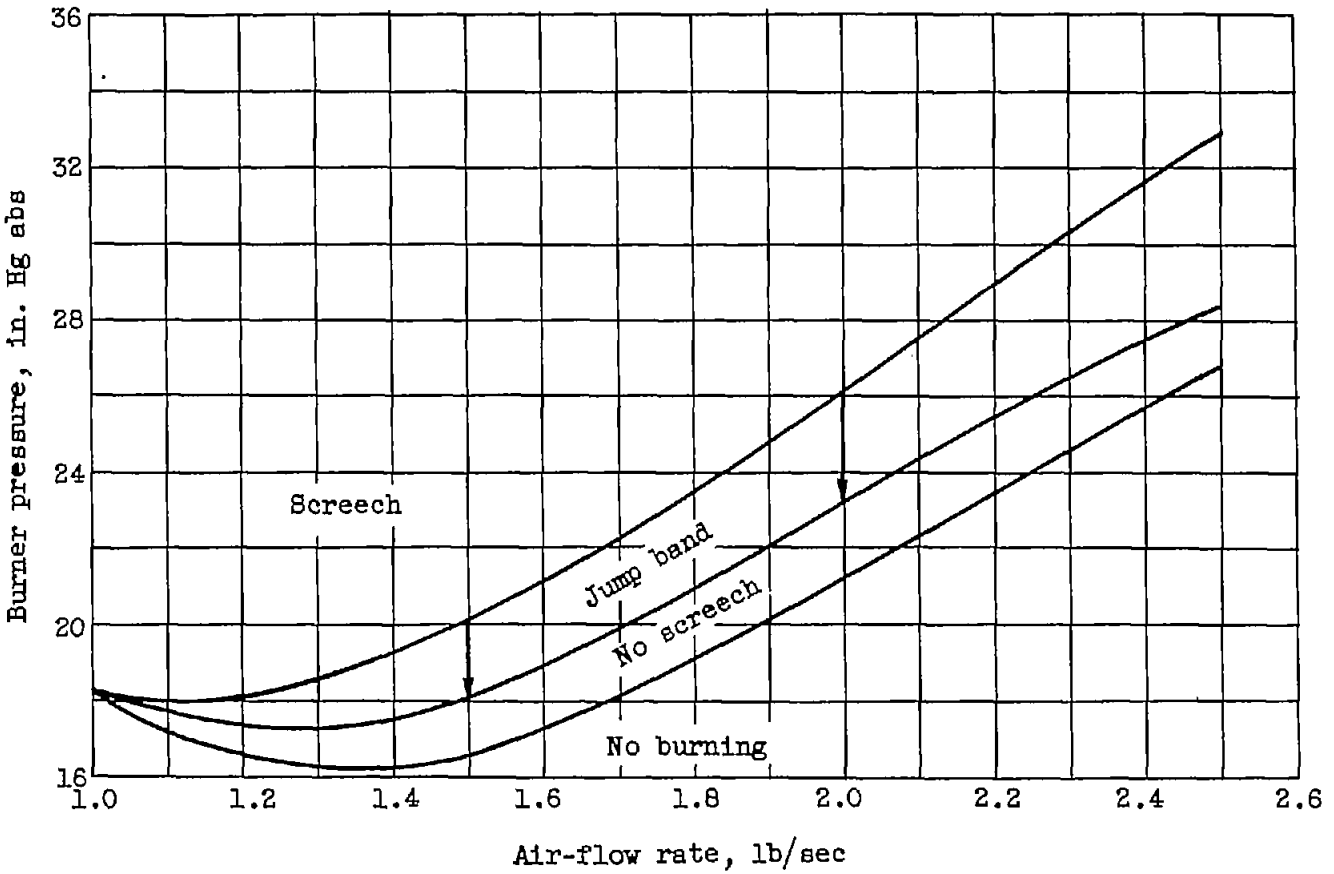

Figure 28. - Lower pressure limits for screech and burning. Equivalence ratio, 1.